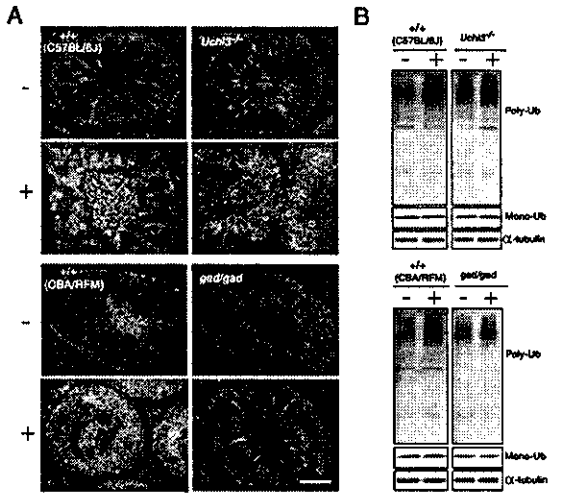

Figure 5. Immunohistochemical and Western blotting analyses of mono- and polyubiquitin in testes on day 7 after experimental cryptorchidism. **A:** Ubiquitin induction was not different between cryptorchid testes from *Uchl3* knockout and wild-type mice, whereas cryptorchid-induced ubiquitin induction in *gad* mice was reduced. Green fluorescence, ubiquitin-positive cells; red fluorescence, nuclei stained with propidium iodide. **B:** Polyubiquitin level in *Uchl3* knockout mice and the two wild-type (C57BL/6J and CBA/RFM) mice substantially increased after injury, whereas that in *gad* mice did not change significantly. Monoubiquitin level did not change after injury. Representative images from four independent experiments are shown (−, scrotal testes; +, cryptorchid testes). Scale bar, 50 μm. Original magnifications, ×200.

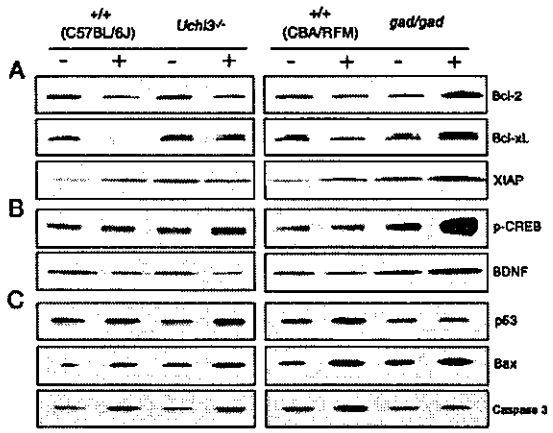

Figure 6. Western blotting analysis of anti-apoptotic, prosurvival, and apoptotic proteins in testes after experimental cryptorchidism. Total protein (5 μg per lane) was prepared from scrotal and cryptorchid testes on day 4 after cryptorchid injury. The expression levels of anti-apoptotic (**A**), prosurvival (**B**), and apoptotic (**C**) proteins in the cryptorchid testes of *Uchl3* knockout, *gad*, and the two wild-type (C57BL/6J and CBA/RFM) mice were significantly different compared with control mice. Representative images from four independent experiments are shown (−, scrotal testes; +, cryptorchid testes).

damage was weaker in the retina of *gad* mice (compared with wild-type mice) after ischemic insult.[17] To determine whether the increase in germ cell apoptosis in cryptorchid testes is associated with ubiquitin induction, we performed immunohistochemical analysis of testes from postoperative day 7 mice. Ubiquitin immunoreactivity increased substantially in cryptorchid testes from *Uchl3* knockout mice and the two wild-type mice, whereas those from *gad* mice showed only minor ubiquitin induction (Figure 5A). The scrotal testes of *Uchl3* knockout and *gad* mice did not show significant differences in ubiquitin induction compared with corresponding controls (Figure 5A). Interestingly, most of the increased ubiquitin induction was detected in spermatocytes and spermatids, consistent with the data on germ cell apoptosis after cryptorchid injury (Figure 3D and Figure 5A). Cryptorchid-induced polyubiquitin levels in the testes from *Uchl3* knockout and the two wild-type mice also increased substantially after injury, whereas the cryptorchid testes of *gad* mice showed no significant difference compared with scrotal testes (Figure 5B); however, the expression levels of monoubiquitin did not change significantly in any of the mice after cryptorchid injury.

Level of Anti-Apoptotic and Apoptotic Proteins in Cryptorchid Uchl3 Knockout and Gad Mice

We previously showed that anti-apoptotic proteins such as Bcl-2 and prosurvival proteins including phosphorylated cyclic AMP response element-binding protein (pCREB) are up-regulated in degenerated retina of *gad* mice.[17] These proteins are degraded by ubiquitination-mediated proteolysis.[30] We examined the expression of the Bcl-2 family proteins, XIAP, pCREB, and caspases to determine their role in testicular germ cell apoptosis after experimental cryptorchidism 4 days after injury in *Uchl3* knockout and *gad* mice. The level of anti-apoptotic proteins such as Bcl-2, Bcl-xL, and XIAP was up-regulated (323.8 ± 57.5, 262.3 ± 22.1, and 209.9 ± 11.7, respectively, as compared with wild type, 100) in the cryptorchid testes of *gad* mice compared with wild-type mice (Figure 6A). Additionally, pCREB, which is normally degraded in a ubiquitination-mediated manner,[30] was apparently highly up-regulated (259.0 ± 22.6, as compared with wild type, 100) in the cryptorchid testes of *gad* mice (Figure 6B). It has been demonstrated that pCREB activates genes that up-regulate trophic factors including BDNF.[31,32] Consistent with pCREB up-regulation, BDNF level also increased (203.0 ± 19.6, as compared with wild type, 100) in cryptorchid testes of *gad* mice (Figure 6B). Level was variable for anti-apoptotic, prosurvival, and apoptotic proteins in the cryptorchid testes of *Uchl3* knockout mice. The level of pCREB, p53, Bax, and caspase3 was slightly increased (169.9 ± 15.2, 152.6 ± 12.9, and 157.3 ± 14.0, respectively, as compared with scrotal testes, 100) in cryptorchid testes of *Uchl3* knockout mice compared with scrotal testes (Figure 6, B and C). Wild-type control mice had a similar expression level pattern except for pCREB. Because p53 acts as an upstream activator of Bax expression,[33] the observed Bax up-regulation after cryptorchid injury was consistent with the elevated p53 level in *Uchl3* knockout and wild-type control mice (Figure 6C). In contrast, BDNF was down-regulated (74.3 ± 7.7 as compared with wild type, 100) in cryptorchid testes of *Uchl3* knockout mice (Figure 6B). The down-regulation of BDNF combined with the up-regulation of pCREB suggests that BDNF might be regulated by another pathway that involves UCH-L3 but not pCREB.[34] Compared with scrotal testes, the expression of anti-apoptotic proteins decreased or was unchanged in cryptorchid testes of *Uchl3* knockout mice (Figure 6A).

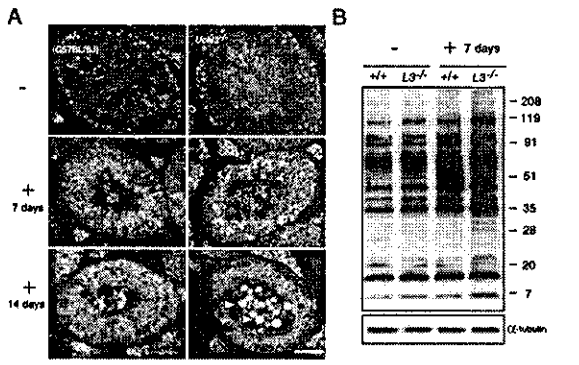

Figure 7. Immunohistochemical and Western blotting analyses of Nedd8 in testes from *Uchl3* knockout mice on days 7 and 14 after experimental cryptorchidism. **A:** Nedd8 induction in *Uchl3* knockout mice increased in both scrotal and cryptorchid testes. The shedding germ cells (**arrowheads**) in the cryptorchid testes of *Uchl3* knockout mice showed strong Nedd8 induction (−, scrotal testes; +7 days and + 4 days, cryptorchid testes). Green fluorescence, Nedd8-positive cells; red fluorescence, nuclei stained with propidium iodide. **B:** On day 7, the expression levels of Nedd8-conjugated proteins in *Uchl3* knockout mice were higher than in wild-type mice. Representative images of four independent experiments are shown. Scale bar, 50 μm. Original magnifications, ×200.

Nedd8 Level in Cryptorchid Uchl3 Knockout Mice

The varied expression levels of ubiquitin, anti-apoptotic, and apoptotic proteins in cryptorchid testes did not adequately explain the relatively exacerbated testicular atrophy and germ cell loss in *Uchl3* knockout mice compared with wild-type mice. We explored the underlying mechanism of this observation using the fact that UCH-L3 cleaves Nedd8.[14,16] We tested whether any change in Nedd8 expression correlated with greater testicular atrophy and germ cell loss in *Uchl3* knockout mice. Nedd8 immunoreactivity was highly detected in scrotal and cryptorchid testes from *Uchl3* knockout mice compared with wild-type mice (Figure 7A). The increased Nedd8 induction was mainly observed in spermatocytes and spermatids, and its expression pattern was similar to that of UCH-L3 during spermatogenesis.[18] These results suggest that Nedd8 may interact closely with UCH-L3 during testicular atrophy and germ cell loss. The cryptorchid testes of *Uchl3* knockout mice showed time-dependent and rapid Nedd8 induction compared with wild-type mice throughout the period 7 to 14 days after injury (Figure 7A). Moreover, the cryptorchid testes of *Uchl3* knockout mice showed strong Nedd8 induction in luminal shedding germ cells on day 14. An immunoblot of scrotal and cryptorchid testes proteins on day 7 confirmed the higher expression levels of Nedd8-conjugated proteins in *Uchl3* knockout mice as compared with wild-type mice (Figure 7B).

Discussion

During spermatogenesis, apoptosis controls germ cell numbers and eliminates defective germ cells to facilitate testicular homeostasis.[35–37] Recent studies indicate that ubiquitination targets proteins for degradation and modulates the turnover of various classes of short-lived signaling proteins.[28,38] Germ cell apoptosis after cryptorchid stress involves genes for various factors, such as Bcl-2 family proteins, p53, and caspases;[39–44] however, the impact of the ubiquitin system on the regulatory mechanisms of germ cell apoptosis is not fully understood. In a previous study, we used *gad* mice, which lack UCH-L1 expression, to show that neural cell apoptosis is suppressed after ischemic retinal injury *in vivo*.[17] These results suggest that UCH-L1 is involved in apoptosis-inducing pathways after stress. UCH-L1 and UCH-L3 are highly similar in sequence; however, UCH-L3 is expressed ubiquitously,[7] whereas UCH-L1 is selectively expressed in neurons and testes/ovaries.[8,9] We recently demonstrated that the expression of these UCH isozymes is differentially and developmentally regulated during spermatogenesis, and that UCH-L1 and UCH-L3 likely have distinct functions during different developmental phases.[18]

To understand the pathophysiological roles of UCH-L1 and UCH-L3 *in vivo*, two mutant mice, *Uchl3* knockout and *gad* mice, were examined after cryptorchid injury. The cryptorchid testes of the two mutant mice had fundamental differences after injury, in that testes of *Uchl3* knockout mice showed profound apoptosis-mediated germ cell loss, whereas *gad* mice were relatively resistant to injury (Figures 3 and 4). In addition, cryptorchid testes of *Uchl3* knockout mice showed greater testicular atrophy and germ cell loss than wild-type mice.

There are several proposed mechanisms for germ cell loss after experimental cryptorchidism.[21–23,45] The tumor suppressor protein, p53, is highly expressed in the testis and regulates both cell proliferation and apoptosis.[23,28,37] A role for p53 in experimental cryptorchidism has been demonstrated convincingly. The higher temperature of the testis caused by cryptorchidism induces p53-mediated apoptosis in the testis, and p53 overexpression results in increased germ cell apoptosis and decreased spermatozoa production.[23,46] In addition to p53, the Bcl-2 family and IAP (inhibitor of apoptosis protein) family are other major classes of intracellular apoptosis regulators.[47,48] The Bcl-2 family can be divided into anti-apoptotic members, such as Bcl-2, Bcl-xL, and Bcl-w, and proapoptotic members, such as Bax and Bak.[49] It has been suggested that the ratio of proapoptotic to anti-apoptotic Bcl-2 family members is important in determining whether a cell will undergo apoptosis.[49] A major function of the Bcl-2 family members appears to be the regulation of mitochondrial events, such as the release of proapoptotic factors.[50] The IAP family inhibits apoptosis primarily by inactivating and degrading proapoptotic proteins.[51] XIAP, a member of IAP family, can bind to and inhibit the proteinase activity of cellular caspase-3 and caspase-9, and thereby block the apoptotic process.[44,52,53]

With regard to cryptorchid injury, the balance between the expression of apoptosis-inducing and apoptosis-protecting proteins constitutes one possible mechanism underlying the observed germ cell apoptosis and protection from apoptosis in *Uchl3* knockout and *gad* mice, respectively. In *gad* mice, cryptorchid injury caused a large increase in the anti-apoptotic proteins Bcl-2, Bcl-xL, and XIAP, consistent with our previous report using retina.[17]

In addition, the expression levels of the prosurvival proteins pCREB and BDNF also increased in *gad* mice. Consistent with these results, caspase-3 expression was suppressed in *gad* mice. Cryptorchid testes of *Uchl3* knockout mice showed slightly increased expression of the apoptotic proteins p53, Bax, and caspase-3 after injury, although similar increases were also observed in wild-type control mice. In total, these results suggest that UCH-L1 plays a role in balancing the expression of apoptosis-inducing and apoptosis-protecting proteins. In contrast, UCH-L3 seems to resist germ cell apoptosis after cryptorchid injury.

Recent studies demonstrate that many molecules in the cellular apoptosis machinery, such as p53,[39,41] Bcl-2 family,[42,43,54] XIAP,[52] and caspase[44] members, are targets for ubiquitination.[28] This suggests that ubiquitination is one of the major mechanisms by which apoptotic cell death is regulated. UCH-L1 has been suggested to associate with monoubiquitin,[13] and the monoubiquitin pool is reduced in *gad* mice relative to wild-type mice. Protection from cryptorchid injury was reported in testes of mice expressing a mutant K48R ubiquitin,[22] suggesting that ubiquitin plays a critical role in processing or modulating testicular insults. Normally, damaged proteins are polyubiquitinated and degraded via the ubiquitin-proteasome system; however, if damaged proteins are not degraded as easily when monoubiquitin is either depleted or mutated, then germ cell death could be delayed.[17,22] Our results with the *gad* mouse suggest that ubiquitin induction plays a critical role in regulating cell death during cryptorchid injury-mediated germ cell apoptosis.

Uchl3 knockout mice exhibit severe retinal degeneration, suggesting that the UCH-L3-mediated ubiquitin pathway is involved in retinal homeostasis.[55] In the cryptorchid testes of *Uchl3* knockout mice, however, the profound testicular weight reduction and germ cell apoptosis after injury cannot be explained by ubiquitin induction alone. Our present results show that *Uchl3* knockout and wild-type mice have similar ubiquitin expression level in the testes, suggesting that UCH-L3 has another nonhydrolase activity in the ubiquitin-proteasome system. UCH-L3 also binds and cleaves the C-terminus of the ubiquitin-like protein, Nedd8.[14,56] This activity is unique to UCH-L3 because UCH-L1 does not cleave Nedd8. Thus, UCH-L3 appears to have dual affinities for ubiquitin and Nedd8. Our present results show that Nedd8 is strongly induced in scrotal testes of *Uchl3* knockout mice compared with those of wild-type mice (Figure 7). Cryptorchid testes of both *Uchl3* knockout and wild-type mice showed Nedd8 induction after injury, although the induction was higher in *Uchl3* knockout mice. These observations suggest that UCH-L3 may function as a deneddylating enzyme[16] *in vivo*, although further studies are necessary to clarify whether UCH-L3 interacts with Nedd8 during spermatogenesis.

In the present study, we demonstrate apparent reciprocal functions for the two deubiquitinating enzymes, UCH-L1 and UCH-L3, with respect to mediating injury after experimental cryptorchidism (Figure 8). Our results advance our understanding of the role of the ubiquitin-proteasome system in regulating apoptosis, and provide a unique opportunity for effective therapeutic intervention.

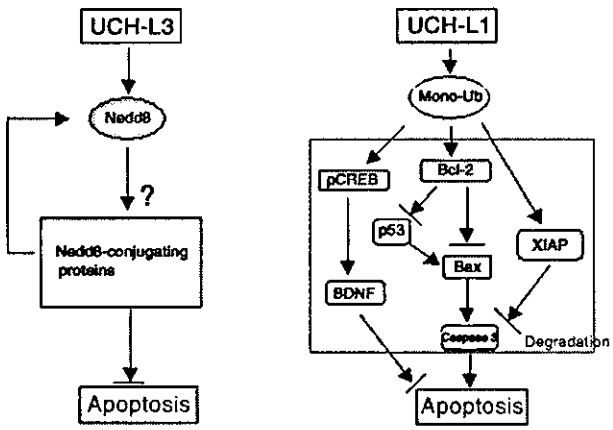

Figure 8. Differential function of the two UCH isozymes in response to experimental cryptorchidism. UCH-L3 has specificity for Nedd8. Cryptorchid injury results in protein damage and the accumulation of Nedd8-conjugated proteins. The accumulation of Nedd8-conjugated proteins in *Uchl3* knockout mice may contribute to profound germ cell loss via apoptosis. Hence, UCH-L3 might function as an anti-apoptotic regulator. UCH-L1 is involved in the maintenance of monoubiquitin levels. A deficiency in monoubiquitin results in delayed polyubiquitination and the accumulation of short-lived proteins after cryptorchid injury. Hence, UCH-L1 may function as a regulator of apoptosis.

Acknowledgments

We thank Dr. S.M. Tilghman for providing *Uchl3* knockout mice, H. Kikuchi for technical assistance with tissue sections, and M. Shikama for the care and breeding of animals.

References

1. Weissman AM: Themes and variations on ubiquitylation. Nat Rev Mol Cell Biol 2001, 2:169–178
2. Ciechanover A: The ubiquitin-proteasome pathway: on protein death and cell life. EMBO J 1998, 17:7151–7160
3. Pickart CM, Rose IA: Ubiquitin carboxyl-terminal hydrolase acts on ubiquitin carboxyl-terminal amides. J Biol Chem 1985, 260:7903–7910
4. Baker RT, Tobias JW, Varshavsky A: Ubiquitin-specific proteases of Saccharomyces cerevisiae. Cloning of UBP2 and UBP3, and functional analysis of the UBP gene family. J Biol Chem 1992, 267:23364–23375
5. Osawa Y, Wang YL, Osaka H, Aoki S, Wada K: Cloning, expression, and mapping of a mouse gene, Uchl4, highly homologous to human and mouse Uchl3. Biochem Biophys Res Commun 2001, 283:627–633
6. Kurihara LJ, Kikuchi T, Wada K, Tilghman SM: Loss of Uch-L1 and Uch-L3 leads to neurodegeneration, posterior paralysis and dysphagia. Hum Mol Genet 2001, 10:1963–1970
7. Kurihara LJ, Semenova E, Levorse JM, Tilghman SM: Expression and functional analysis of Uch-L3 during mouse development. Mol Cell Biol 2000, 20:2498–2504
8. Saigoh K, Wang YL, Suh JG, Yamanishi T, Sakai Y, Kiyosawa H, Harada T, Ichihara N, Wakana S, Kikuchi T, Wada K: Intragenic deletion in the gene encoding ubiquitin carboxy-terminal hydrolase in gad mice. Nat Genet 1999, 23:47–51
9. Kon Y, Endoh D, Iwanaga T: Expression of protein gene product 9.5, a neuronal ubiquitin C-terminal hydrolase, and its developing change in Sertoli cells of mouse testis. Mol Reprod Dev 1999, 54:333–341
10. Wilkinson KD, Deshpande S, Larsen CN: Comparisons of neuronal (PGP 9.5) and non-neuronal ubiquitin C-terminal hydrolases. Biochem Soc Trans 1992, 20:631–637
11. Liu Y, Fallon L, Lashuel HA, Liu Z, Lansbury Jr PT: The UCH-L1 gene

encodes two opposing enzymatic activities that affect alpha-synuclein degradation and Parkinson's disease susceptibility. Cell 2002, 111:209–218
12. Liu Y, Lashuel HA, Choi S, Xing X, Case A, Ni J, Yeh LA, Cuny GD, Stein RL, Lansbury Jr PT: Discovery of inhibitors that elucidate the role of UCH-L1 activity in the H1299 lung cancer cell line. Chem Biol 2003, 10:837–846
13. Osaka H, Wang YL, Takada K, Takizawa S, Setsuie R, Li H, Sato Y, Nishikawa K, Sun YJ, Sakurai M, Harada T, Hara Y, Kimura I, Chiba S, Namikawa K, Kiyama H, Noda M, Aoki S, Wada K: Ubiquitin carboxy-terminal hydrolase L1 binds to and stabilizes monoubiquitin in neuron. Hum Mol Genet 2003, 12:1945–1958
14. Wada H, Kito K, Caskey LS, Yeh ET, Kamitani T: Cleavage of the C-terminus of NEDD8 by UCH-L3. Biochem Biophys Res Commun 1998, 251:688–692
15. Hemelaar J, Borodovsky A, Kessler BM, Reverter D, Cook J, Kolli N, Gan-Erdene T, Wilkinson KD, Gill G, Lima CD, Ploegh HL, Ovaa H: Specific and covalent targeting of conjugating and deconjugating enzymes of ubiquitin-like proteins. Mol Cell Biol 2004, 24:84–95
16. Gong L, Kamitani T, Millas S, Yeh ET: Identification of a novel isopeptidase with dual specificity for ubiquitin- and NEDD8-conjugated proteins. J Biol Chem 2000, 275:14212–14216
17. Harada T, Harada C, Wang YL, Osaka H, Amanai K, Tanaka K, Takizawa S, Setsuie R, Sakurai M, Sato Y, Noda M, Wada K: Role of ubiquitin carboxy terminal hydrolase-L1 in neural cell apoptosis induced by ischemic retinal injury in vivo. Am J Pathol 2004, 164:59–64
18. Kwon J, Wang YL, Setsuie R, Sekiguchi S, Sakurai M, Sato Y, Lee WW, Ishii Y, Kyuwa S, Noda M, Wada K, Yoshikawa Y: Developmental regulation of ubiquitin C-terminal hydrolase isozyme expression during spermatogenesis in mice. Biol Reprod 2004, 71:515–521
19. Boekelheide K, Hall SJ: 2,5-Hexanedione exposure in the rat results in long-term testicular atrophy despite the presence of residual spermatogonia. J Androl 1991, 12:18–26
20. Ohta Y, Nishikawa A, Fukazawa Y, Urushitani H, Matsuzawa A, Nishina Y, Iguchi T: Apoptosis in adult mouse testis induced by experimental cryptorchidism. Acta Anat (Basel) 1996, 157:195–204
21. Yin Y, Hawkins KL, DeWolf WC, Morgentaler A: Heat stress causes testicular germ cell apoptosis in adult mice. J Androl 1997, 18:159–165
22. Rasoulpour RJ, Schoenfeld HA, Gray DA, Boekelheide K: Expression of a K48R mutant ubiquitin protects mouse testis from cryptorchid injury and aging. Am J Pathol 2003, 163:2595–2603
23. Yin Y, DeWolf WC, Morgentaler A: Experimental cryptorchidism induces testicular germ cell apoptosis by p53-dependent and -independent pathways in mice. Biol Reprod 1998, 58:492–496
24. Peltola V, Huhtaniemi I, Ahotupa M: Abdominal position of the rat testis is associated with high level of lipid peroxidation. Biol Reprod 1995, 53:1146–1150
25. Ahotupa M, Huhtaniemi I: Impaired detoxification of reactive oxygen and consequent oxidative stress in experimentally cryptorchid rat testis. Biol Reprod 1992, 46:1114–1118
26. Morimoto RI, Santoro MG: Stress-inducible responses and heat shock proteins: new pharmacologic targets for cytoprotection. Nature Biotechnol 1998, 16:833–838
27. Wojcik C: Proteasomes in apoptosis: villains or guardians? Cell Mol Life Sci 1999, 56:908–917
28. Yang Y, Yu X: Regulation of apoptosis: the ubiquitous way. EMBO J 2003, 17:790–799
29. Kwon J, Kikuchi T, Setsuie R, Ishii Y, Kyuwa S, Yoshikawa Y: Characterization of the testis in congenitally ubiquitin carboxy-terminal hydrolase-1 (Uch-L1) defective (gad) mice. Exp Anim 2003, 52:1–9
30. Taylor CT, Furuta GT, Synnestvedt K, Colgan SP: Phosphorylation-dependent targeting of cAMP response element binding protein to the ubiquitin/proteasome pathway in hypoxia. Proc Natl Acad Sci USA 2000, 97:12091–12096
31. Park C, Choi WS, Kwon H, Kwon YK: Temporal and spatial expression of neurotrophins and their receptors during male germ cell development. Mol Cells 2001, 12:360–367
32. Finkbeiner S: CREB couples neurotrophin signals to survival messages. Neuron 2000, 25:11–14
33. Selvakumaran M, Lin HK, Miyashita T, Wang HG, Krajewski S, Reed JC, Hoffman B, Liebermann D: Immediate early up-regulation of bax expression by p53 but not TGF beta 1: a paradigm for distinct apoptotic pathways. Oncogene 1994, 9:1791–1798
34. Liu L, Cavanaugh JE, Wang Y, Sakagami H, Mao Z, Xia Z: ERK5 activation of MEF2-mediated gene expression plays a critical role in BDNF-promoted survival of developing but not mature cortical neurons. Proc Natl Acad Sci USA 2003, 100:8532–8537
35. Matsui Y: Regulation of germ cell death in mammalian gonads. APMIS 1998, 106:142–148
36. Gosden R, Spears N: Programmed cell death in the reproductive system. Br Med Bull 1997, 53:644–661
37. Print CG, Loveland KL: Germ cell suicide: new insights into apoptosis during spermatogenesis. Bioessays 2000, 22:423–430
38. Lee JC, Peter ME: Regulation of apoptosis by ubiquitination. Immunol Rev 2003, 193:39–47
39. Haupt Y, Maya R, Kazaz A, Oren M: Mdm2 promotes the rapid degradation of p53. Nature 1997, 387:296–299
40. Oren M: Regulation of the p53 tumor suppressor protein. J Biol Chem 1999, 274:36031–36034
41. Ryan KM, Phillips AC, Vousden KH: Regulation and function of the p53 tumor suppressor protein. Curr Opin Cell Biol 2001, 13:332–337
42. Dimmeler S, Breitschopf K, Haendeler J, Zeiher AM: Dephosphorylation targets Bcl-2 for ubiquitin-dependent degradation: a link between the apoptosome and the proteasome pathway. J Exp Med 1999, 189:1815–1822
43. Marshansky V, Wang X, Bertrand R, Luo H, Duguid W, Chinnadurai G, Kanaan N, Vu MD, Wu J: Proteasomes modulate balance among proapoptotic and antiapoptotic Bcl-2 family members and compromise functioning of the electron transport chain in leukemic cells. J Immunol 2001, 166:3130–3142
44. Suzuki Y, Nakabayashi Y, Takahashi R: Ubiquitin-protein ligase activity of X-linked inhibitor of apoptosis protein promotes proteasomal degradation of caspase-3 and enhances its anti-apoptotic effect in Fas-induced cell death. Proc Natl Acad Sci USA 2001, 98:8662–8667
45. Yin Y, Stahl BC, DeWolf WC, Morgentaler A: P53 and Fas are sequential mechanisms of testicular germ cell apoptosis. J Androl 2002, 23:64–70
46. Ohta H, Aizawa S, Nishimune Y: Functional analysis of the p53 gene in apoptosis induced by heat stress or loss of stem cell factor signaling in mouse male germ cells. Biol Reprod 2003, 68:2249–2254
47. Beumer TL, Roepers-Gajadien HL, Gademan IS, Lock TM, Kal HB, De Rooij DG: Apoptosis regulation in the testis: involvement of Bcl-2 family members. Mol Reprod Dev 2000, 56:353–359
48. Oldereid NB, Angelis PD, Wiger R, Clausen OP: Expression of Bcl-2 family proteins and spontaneous apoptosis in normal human testis. Mol Hum Reprod 2001, 7:403–408
49. Borner C: The Bcl-2 protein family: sensors and checkpoints for life-or-death decisions. Mol Immunol 2003, 39:615–647
50. Yamamoto CM, Sinha Hikim AP, Huynh PN, Shapiro B, Lue Y, Salameh WA, Wang C, Swerdloff RS: Redistribution of Bax is an early step in an apoptotic pathway leading to germ cell death in rats, triggered by mild testicular hyperthermia. Biol Reprod 2000, 63: 1683–1690
51. Deveraux QL, Reed JC: IAP family proteins—suppressors of apoptosis. Genes Dev 1999, 13:239–252
52. Yang Y, Fang S, Jensen JP, Weissman AM, Ashwell JD: Ubiquitin protein ligase activity of IAPs and their degradation in proteasomes in response to apoptotic stimuli. Science 2000, 288:874–877
53. Deveraux QL, Roy N, Stennicke HR, Van Arsdale T, Zhou Q, Srinivasula SM, Alnemri ES, Salvesen GS, Reed JC: IAPs block apoptotic events induced by caspase-8 and cytochrome c by direct inhibition of distinct caspases. EMBO J 1998, 17:2215–2223
54. Li B, Dou QP: Bax degradation by the ubiquitin/proteasome-dependent pathway: involvement in tumor survival and progression. Proc Natl Acad Sci USA 2000, 97:3850–3855
55. Semenova E, Wang X, Jablonski MM, Levorse J, Tilghman SM: An engineered 800 kilobase deletion of Uchl3 and Lmo7 on mouse chromosome 14 causes defects in viability, postnatal growth and degeneration of muscle and retina. Hum Mol Genet 2003, 12:1301–1312
56. Dil Kuazi A, Kito K, Abe Y, Shin RW, Kamitani T, Ueda N: NEDD8 protein is involved in ubiquitinated inclusion bodies. J Pathol 2003, 199:259–266

doi:10.1093/brain/awh368 *Brain* (2005), **128**, 405–416

The slow Wallerian degeneration gene, *Wld*^{S}, inhibits axonal spheroid pathology in gracile axonal dystrophy mice

Weiqian Mi,[1,*] Bogdan Beirowski,[1,2,*] Thomas H. Gillingwater,[3] Robert Adalbert,[1,4] Diana Wagner,[1] Daniela Grumme,[1] Hitoshi Osaka,[5,6] Laura Conforti,[4] Stefan Arnhold,[2] Klaus Addicks,[2] Keiji Wada,[5] Richard R. Ribchester[3] and Michael P. Coleman[1,4]

[1]*ZMMK and Institute for Genetics and* [2]*Department of Anatomy I, University of Cologne, Cologne, Germany,* [3]*Division of Neuroscience, University of Edinburgh, Edinburgh,* [4]*The Babraham Institute, Babraham, Cambridge, UK,* [5]*Department of Degenerative Neurological Diseases, National Institute of Neuroscience, Kodaira, Tokyo and* [6]*Clinical Research Institute, Kanagawa Children's Medical Center, Yokohama, Japan*

Correspondence: Dr Michael Coleman, The Babraham Institute, Babraham, Cambridge CB2 4AT, UK
E-mail: michael.coleman@bbsrc.ac.uk
**W. Mi and B. Beirowski contributed equally to this work*

Summary

Axonal dystrophy is the hallmark of axon pathology in many neurodegenerative disorders of the CNS, including Alzheimer's disease, Parkinson's disease and stroke. Axons can also form larger swellings, or spheroids, as in multiple sclerosis and traumatic brain injury. Some spheroids are terminal endbulbs of axon stumps, but swellings may also occur on unbroken axons and their role in axon loss remains uncertain. Similarly, it is not known whether spheroids and axonal dystrophy in so many different CNS disorders arise by a common mechanism. These surprising gaps in current knowledge result largely from the lack of experimental methods to manipulate axon pathology. The slow Wallerian degeneration gene, *Wld*^{S}, delays Wallerian degeneration after injury, and also delays 'dying-back' in peripheral nervous system disorders, revealing a mechanistic link between two forms of axon degeneration traditionally considered distinct. We now report that *Wld*^{S} also inhibits axonal spheroid pathology in gracile axonal dystrophy (*gad*) mice. Both gracile nucleus ($P < 0.001$) and cervical gracile fascicle ($P = 0.001$) contained significantly fewer spheroids in *gad*/*Wld*^{S} mice, and secondary signs of axon pathology such as myelin loss were also reduced. Motor nerve terminals at neuromuscular junctions continued to degenerate in *gad*/*Wld*^{S} mice, consistent with previous observations that *Wld*^{S} has a weaker effect on synapses than on axons, and probably contributing to the fact that *Wld*^{S} did not alleviate *gad* symptoms. *Wld*^{S} acts downstream of the initial pathogenic events to block *gad* pathology, suggesting that its effect on axonal swelling need not be specific to this disease. We conclude that axon degeneration mechanisms are more closely related than previously thought and that a link exists in *gad* between spheroid pathology and Wallerian degeneration that could hold for other disorders.

Keywords: axon; axonal spheroid; gracile axonal dystrophy; ubiquitin; Wallerian degeneration

Abbreviations: APP = amyloid precursor protein; *gad* = gracile axonal dystrophy; GFAP = glial fibrillary acidic protein; H & E = haematoxylin and eosin; NMJ = neuromuscular junction; PFA = paraformaldehyde; PNS = peripheral nervous system; *Wld*^{S} = slow Wallerian degeneration gene, mutation or mice; Wld^S = slow Wallerian degeneration protein; YFP = yellow fluorescent protein

Received April 17, 2004. Revised August 12, 2004. Accepted November 1, 2004. Advance Access publication January 11, 2005

Introduction

Axonal dystrophy and spheroids are hallmarks of CNS axon pathology. Axonal spheroids are focal 10–50 μm diameter swellings, which are sometimes, but not always, terminal endbulbs, and are filled with disorganized neurofilaments,

tubules, organelles or multi-lamellar inclusions. Dystrophic axons are usually smaller swellings often associated with continuity of the axon. One or both of these aberrant axon morphologies is found in a wide range of CNS neurodegenerative disorders, including stroke (Dewar *et al.*, 1999), myelin disorders (Griffiths *et al.*, 1998), tauopathies (Lewis *et al.*, 2000; Probst *et al.*, 2000), amyotrophic lateral sclerosis (Tu *et al.*, 1996; Oosthuyse *et al.*, 2001; Howland *et al.*, 2002), traumatic brain injury (Cheng and Povlishock, 1988), Alzheimer's disease (Brendza *et al.*, 2003), Parkinson's disease (Galvin *et al.*, 1999), Creutzfeldt–Jakob disease (Liberski and Budka, 1999), HIV dementia (Raja *et al.*, 1997; Adle-Biassette *et al.*, 1999), hereditary spastic paraplegia (Ferreirinha *et al.*, 2004) and Niemann–Pick disease (Bu *et al.*, 2002). They also occur during normal ageing and secondarily in some serious illnesses (Sung *et al.*, 1981). In contrast, peripheral nervous system (PNS) axons undergo 'Wallerian-like' or 'dying-back' degeneration, even in diseases where CNS axons form swellings (Miura *et al.*, 1993; Lewis *et al.*, 2000; Oosthuyse *et al.*, 2001), although swellings do also occur in some rare PNS disorders (Miike *et al.*, 1986; Bomont *et al.*, 2000).

The roles of axonal swellings in disease are poorly understood, as illustrated by the following examples. First, in multiple sclerosis, many large spheroids are terminal endbulbs of transected axons but there are also a few 'en passant' swellings of similar shape and dimension (Trapp *et al.*, 1998) and many small dystrophic swellings (Ferguson *et al.*, 1997; Kornek *et al.*, 2000, 2001). It remains unclear whether these different types of swelling have common or different origins. Secondly, it is not clear whether disease-specific mechanisms lead to a common final pathway of axonal dystrophy, as in Alzheimer's disease, stroke and multiple sclerosis, and if so how they do this. Thirdly, it is not known why swellings predominate in distal axons in some diseases, such as gracile axonal dystrophy (*gad*) (Yamazaki *et al.*, 1988; Mukoyama *et al.*, 1989), caused by loss of ubiquitin C-terminal hydrolase 11 (*Uch-l1*) (Saigoh *et al.*, 1999), while in other diseases they occur in proximal axons, as in amyotrophic lateral sclerosis (Tu *et al.*, 1996) and tauopathy (Probst *et al.*, 2000). Finally, a better understanding is needed of the relationship between axon swelling and impaired axonal transport. Amyloid precursor protein (APP) accumulates in axonal swellings and spheroids in stroke (Dewar *et al.*, 1999), traumatic brain injury (Gentleman *et al.*, 1993), multiple sclerosis (Ferguson *et al.*, 1997), Creutzfeld–Jakob disease (Liberski and Budka, 1999), HIV dementia (Raja *et al.*, 1997; Adle-Biassette *et al.*, 1999) and *gad* (Ichihara *et al.*, 1995), indicating that axonal transport is impaired. However, it is not known whether axon swelling in these disorders is simply a consequence of impaired axonal transport, or whether it causes the transport defect, or both. These and other important questions remain unanswered largely because experimental methods to manipulate axonal swelling have not been available.

A mutant mouse gene, Wld^S, blocks a rate-limiting step common to Wallerian degeneration and diverse PNS axon disorders, including dysmyelination (Samsam *et al.*, 2003), motor neuronopathy (Ferri *et al.*, 2003) and Taxol toxicity (Wang *et al.*, 2002). Recently, Wld^S was reported to be effective in acute CNS lesions modelling stroke (Gillingwater *et al.*, 2004) and Parkinson's disease (Sajadi *et al.*, 2004) but its effect in a chronic CNS disease has not been reported. Wld^S is a chimeric gene (Conforti *et al.*, 2000) formed by a stable triplication (Coleman *et al.*, 1998; Mi *et al.*, 2003) encoding the N-terminus of multiubiquitylation factor Ube4b fused in-frame to nicotinamide mononucleotide adenylyltransferase (Nmnat1) plus a short novel sequence (Mack *et al.*, 2001). Nmnat1 appears to be sufficient to confer the phenotype *in vitro*, but it is not yet clear whether this holds *in vivo* (Coleman and Perry, 2002; Araki *et al.*, 2004). Wld^S protein appears to be restricted to the nucleus, so its effect on axons is mediated by other factors (Mack *et al.*, 2001), which may include the NAD-dependent deacetylase SIRT-1 (Araki *et al.*, 2004).

To study the relationship between axonal swelling and Wallerian degeneration, we crossed Wld^S and *gad* mice. Wld^S significantly reduced spheroid numbers without altering the first stages of *gad* pathogenesis, revealing a link between Wallerian degeneration and axonal spheroids in this disease that could extend to other disorders.

Methods

Origin, breeding and genotyping of mice

Homozygous C57BL/Wld^S spontaneous mutants were obtained from Harlan UK (Bicester, UK) and mated with heterozygous *gad* mice, kindly provided by Professor Keiji Wada and Dr Hitoshi Osaka (National Institute of Neuroscience, Tokyo, Japan), following a cross to C57BL/6 to ensure a more homogeneous genetic background. Thus, the genetic background of the experimental mice was 75% C57BL/6, 12.5% CBA/Nga, 12.5% RFM/Nga. Double heterozygotes were identified in the F1 generation by genotyping for *gad* (below) and intercrossed. *gad* homozygotes were identified by genotyping and selected for further study. Wld^S genotype was determined *post mortem* by pulsed-field gel electrophoresis of spleen DNA (Mi *et al.*, 2002). Hemizygous yellow fluorescent protein (YFP) mice of line YFP-H were obtained from Jackson Laboratories (Bar Harbor, MN, USA) and mated with *gad*/Wld^S double heterozygotes. Triple heterozygotes were then mated to *gad*/Wld^S double heterozygotes to produce *gad* homozygotes that were heterozygous for both Wld^S and YFP-H. For *gad* genotyping, tail genomic DNA was extracted at 3 weeks using the Nucleon II kit (Amersham Pharmacia), digested with *Pvu*II, and Southern blotted. It was then hybridized with a ^{32}P-labelled 764-bp probe generated by PCR from *gad* homozygous genomic DNA using primers 5′-ATCCAGGCGGCCCATGACTC-3′ and 5′-AGCTGCTTTGCAGAGAGCCA-3′. Positively hybridizing fragments indicative of the *gad* (0.75 kb) and wild-type (1.6 kb) alleles were then identified by autoradiography. To genotype for inheritance of the YFP-H transgene, the skin of a 1–2 mm ear punch at 21 days was pulled apart and fluorescent axons identified using a Zeiss Axiovert S100 inverted fluorescent microscope through the FITC filter.

Assessment of Wallerian degeneration

gad homozygotes that were heterozygous for *Wld*^{S} and hemizygous for the *YFP-H* transgene were anaesthetized prior to the onset of hindlimb weakness using intraperitoneal Ketanest (100 mg/kg; Parke Davis/Pfizer, Karlsruhe, Germany) and Rompun (5 mg/kg; Bayer, Leverkusen, Germany). The right sciatic nerve (upper thigh) was transected and the wound closed with a single suture. Five days later the mice were killed by cervical dislocation, the swollen first 2 mm of distal sciatic nerve was discarded and the next 2 mm was used for western blotting for heavy neurofilament protein as previously described (Mack *et al.*, 2001). The tibial nerve of the operated leg with a minimum of attached non-nervous tissue was processed for YFP fluorescence as follows. The nerve was stretched by ~10% by pinning onto a Sylgard (Du Pont) dish and fixed with 4% paraformaldehyde (PFA) (BDH Laboratory, UK) in 0.1 M phosphate-buffered saline (PBS) in the dark for 1 h. It was then incubated in 1% Triton X-100 (Sigma, Germany) in 0.1 M PBS for 10 min and washed three times with PBS before mounting in Vectashield (Vector Laboratories, USA). The degree of fragmentation of the representative subset of motor and sensory axons that are YFP-labelled was determined. For more detail, see Beirowski *et al.* (2004).

Preparation of gracile tract sections

Mice aged 126–130 days were anaesthetized using Ketanest and Rompun (100 mg/kg and 5 mg/kg intraperitoneally, respectively) or a higher dose as required for deep terminal anaesthesia. After sternotomy mice were killed by cardiac puncture and instantly intracardially perfused first with a solution containing 10 000 IE/l heparin (Liquemin N 25000; Hoffmann-La Roche) and 1% procainhydrochloride in 0.1 M PBS for 30 s and then with fixative (4% paraformaldehyde in 0.1 M PBS) for 10 min. Brain and spinal cord were carefully removed, further fixed in 4% PFA/0.1 M PBS overnight and extensively washed in 0.1 M PBS. Fixed tissues were extensively rinsed in fresh 0.1 M PBS, dehydrated in an ascending ethanol series and subsequently embedded in paraffin (Paraplast; Sherwood Medical Co., St Louis, MO, USA) applying standard histology techniques. Coronal serial sections (6 µm) were made using a Type HM355 microtome (Microm GmbH) from the entire gracile nucleus in medulla oblongata and cervical gracile fascicle starting at level 535 (Sidman *et al.*, 1971). Serial paraffin sections were mounted on conventional glass slides for use in haematoxylin and eosin (H & E) staining or on poly-L-lysine-coated slides for use in Luxol Fast Blue staining and immunocytochemistry, alternating normally every 2–3 sections. Distinction between gracile nucleus and cervical gracile fascicle was made by applying histomorphological criteria for the typical shapes of coronal sections.

H & E staining and spheroid quantification

Six-micrometre sections were deparaffinized in xylol (Carl-Roth, Germany) for 10 min, rehydrated in a descending ethanol series and rinsed in deionized H_2O for 1 min. Sections were placed in haematoxylin for 5 min, rinsed in tap water for 1 min to allow stain to develop and then placed in eosin for 2 min, dehydrated and mounted in Entellan resin (Merck, Germany). The occurrence of clearly detectable eosinophilic spheroids, indicative of dystrophic axons (Yamazaki *et al.*, 1988; Mukoyama *et al.*, 1989; Kikuchi *et al.*, 1990) was quantified in ~90 sections uniformly dispersed throughout the gracile nucleus of each individual and ~30 sections uniformly dispersed throughout the cervical gracile fascicle. Analysis of lateral columns was performed on these same 30 sections, counting the sum of spheroid numbers on both sides of the spinal cord. In this way, irregular results due to local deviations in spheroid numbers could be ruled out. H & E stained axonal spheroids were generally eosinophilic and appeared glassy or hyaline with a round or oval shape. They varied in diameter (5–50 µm) and sometimes reached a size larger than the nerve cells in gracile nucleus. All specimens were scored blind and agreed by two independent investigators.

Luxol Fast Blue staining and densitometric quantification

Six-micrometre sections from equivalent points in *gad* and *gad/Wld*^{S} cervical spinal cord and medulla oblongata were processed simultaneously as follows. Sections were deparaffinized in xylol (Carl-Roth, Germany) for 15 min, and processed twice through 100% ethanol for 2 min and 96% ethanol for a few seconds. Slides were transferred to Luxol Fast Blue solution [0.1% Luxol Fast Blue MBS chroma (Merck), 10% acetic acid all made up in 96% ethanol] and incubated at 60°C for 5 h. Sections were then rinsed in 95% ethanol and distilled water for 1 min each, dipped in 0.05% lithium carbonate (Merck) for 1 min, and differentiated in 70% ethanol for a further 1 min. After rinsing in distilled water, sections were examined under light microscope for suitable differentiation between white and grey matter. Nuclear Fast Red staining was carried out for 10 min in 5% aluminium sulphate, 0.1% Nuclear Fast Red followed by rinsing in distilled H_2O, 90% ethanol and 100% ethanol for 1 min each. Slides were incubated in xylol for 5 min and mounted in Entellan resin (Merck). Slides were examined under light microscopy (Nikon Eclipse E200) and evaluated using Bioscan OPTIMAS 6.0 software (Optimas Corp., WA, USA) according to the manufacturer's instructions. For densitometric quantitation, mean grey values were obtained for circumscribed areas of interest using a three-chip monochrome CCD camera, and the background grey value (tissue-free area) was subtracted. Since demyelination occurs selectively in the gracile tract and not in the cuneate tract of *gad* mice by 126–130 days (Mukoyama *et al.*, 1989; our observations), we used cuneate fascicle as a reference area and expressed Luxol Fast Blue staining in gracile tract as a percentage of that in cuneate tract. We applied this procedure to representative Luxol Fast Blue-stained sections of cranial gracile tract: two sections from level C2/C3 representing the cervical gracile fascicle and two sections from level 535 representing the gracile nucleus (Sidman *et al.*, 1971).

Immunocytochemistry of gracile tract

Six-micrometre paraffin sections from equivalent points in *gad* and *gad/Wld*^{S} cervical spinal cord and medulla oblongata were processed simultaneously as follows. Sections were deparaffinized, rehydrated in a descending ethanol series, washed several times in 0.05 M Tris-buffered saline (TBS), and treated with a solution of 6% H_2O_2 in methanol for 20 min to block endogenous peroxidase activity. They were then permeabilized with 0.1% Triton X-100 (Sigma) in 0.05 M TBS additionally containing 0.05 M NH_4Cl, rinsed in fresh TBS three times and subsequently immunoblocked with 5% bovine serum albumin (Sigma) in 0.05 M TBS

for 1 h. First antibody was polyclonal guinea pig anti-glial fibrillary acidic protein (GFAP) (1 : 400 dilution) (Progen, Germany) at 4°C overnight, while negative control sections were incubated without primary antibody. Secondary antibody was goat anti-guinea pig biotin conjugate (1 : 400 dilution) (Sigma) for 1 h at room temperature, and was followed by streptavidin-coupled horseradish peroxidase complex (Vector Laboratories; 1 : 200 dilution) for 1 h. After extensive washing, sections were developed under identical conditions for all specimens with 3,3-diaminobenzidine tetrahydrochloride (Sigma–Aldrich) in 0.1 M phosphate buffer until a clear dark-brown labelling of astrocytes in the gracile tract could be detected. In all cases the control sections without primary antibody incubation showed no labelling of astrocytes. For microscopic examination and TV densitometry, sections were dehydrated and mounted in Entellan resin (Merck). Quantitation was similar to that described for Luxol Fast Blue densitometry. GFAP immunostaining intensities in cranial gracile tract sections were expressed as percentage of GFAP staining intensity in wild-type sections at the same coronal level. We applied GFAP densitometry on representative cranial gracile tract sections from each examined mouse: two sections from level C2/C3 representing the cervical gracile fascicle and two sections from level 535 representing the gracile nucleus (Sidman *et al.*, 1971).

Immunocytochemistry of sciatic nerves

Sciatic nerves from 15-week-old *gad*, *gad/Wld*^{S}, or control mice were immersion fixed in 4% PFA/0.1 M PBS for 1 h and washed extensively in 0.1 M PBS before paraffin embedding. Twenty-micrometre sections were immunostained using rabbit polyclonal antibody to ubiquitin (Sigma–Aldrich U5379) and Cy3-conjugated secondary antibody. Confocal images were obtained using a PerkinElmer UltraView LCI confocal microscope coupled to a Nikon Eclipse TE200 microscope, and processed using UltraView software (Perkin-Elmer Life Sciences Ltd, Cambridge, UK).

Statistical analysis of histopathology results

All data (axonal spheroid numbers, TV densitometry intensities) are presented as mean ± SD for the examined genotype groups. Data analysis was performed using PRISM for Macintosh or SPSS for Windows, including Student's *t*-test calculations for paired and unpaired data where appropriate. Significance was considered at $P < 0.05$ and high significance at a $P < 0.01$.

Analysis of neuromuscular pathology

Mice were killed by cervical dislocation and lumbrical muscles immediately dissected under oxygenated Ringer solution. Fixation, immunocytochemistry and signal imaging were then carried out as described previously (Gillingwater *et al.*, 2002). The denervation rate was determined by counting 100–200 endplates in each of two to three lumbrical muscles and the mean value taken for each mouse.

Behavioural tests

The foot splay test (Norreel *et al.*, 2001) was used to estimate the reflex reaction speed of the hind limbs. Mice were gently taken by the neck and tail, the plantar surface of their hind feet painted using a non-toxic children's painting set, and the mouse released from a height of 15 cm to land on white paper. Wild-type mice bring their legs together during descent to land in a controlled manner like a gymnast, whereas *gad* mice fail to do this and land with their feet far apart. The distance between the two hind heels was averaged from 10 successive trials on each testing date (9 and 13 weeks).

In the clasping test, the mouse was suspended by the tail >50 cm from any surface. Clasping time within a 1 min test was scored as flexing or folding of the hind limbs tightly towards the trunk plus any spasmodic stretching. Mice were examined once per week through the period from 6 to 16 weeks. No wild-type mice clasped, regardless of the presence of the *Wld*^{S} mutation.

Results

gad does not weaken the Wld^S *phenotype*

Before assessing the effect of *Wld*^{S} on *gad* pathology we first showed that *Wld*^{S} can protect axons, even in the presence of the *gad* mutation, by inducing Wallerian degeneration in *gad/Wld*^{S} mice. Before the lesion, there was no sign of axon degeneration in these nerves, confirming previous reports (Mukoyama *et al.*, 1989). We bred *gad* mice that were heterozygous for *Wld*^{S} and hemizygous for a *YFP-H* transgene (Feng *et al.*, 2000) to allow a rapid and quantitative assessment of Wallerian degeneration (Beirowski *et al.*, 2004) and transected sciatic nerves before the onset of hindlimb weakness. Wallerian degeneration was assessed after 5 days both by western blotting to see degraded heavy neurofilament protein (Fig. 1A) and by fluorescence microscopy to see fragmented YFP-containing axons (Fig. 1B). Nerves unprotected by *Wld*^{S} degenerated as expected (Fig. 1A, middle lane, and Fig. 1B, lower panel) but a single allele of *Wld*^{S} was sufficient to prevent axon degeneration in both readout methods. Thus, *gad* does not significantly weaken the *Wld*^{S} phenotype and it is feasible to test the effect of *Wld*^{S} on *gad* pathology.

Axonal spheroid pathology is reduced by Wld^S

In order to determine the effectiveness of *Wld*^{S} on *gad* axonal spheroid pathology, we counted axonal spheroids in ~90 H & E stained 6-μm paraffin sections from throughout the gracile nucleus and 30 sections from throughout the cervical spinal cord of each 18-week-old *gad* mouse and *gad/Wld*^{S} double homozygote. Fifty per cent fewer spheroids were found in gracile nuclei of *gad/Wld*^{S} mice than in *gad* mice ($P = 0.0004$) and 63% fewer in cervical gracile fascicle ($P = 0.0011$) (Fig. 2). Intermediate values were observed in *Wld*^{S} heterozygotes, further supporting the result and no spheroids were observed in control animals of this age (data not shown). Spheroids have also been reported in the cervical lateral columns of *gad* mice (Kikuchi *et al.*, 1990). We found far fewer spheroids here than in cervical gracile tract and gracile nucleus, but the number was also significantly reduced by homozygous *Wld*^{S} ($P = 0.046$; $n = 3$) (Fig. 2). We also observed a reduction in axonal spheroids in lumbar spinal cord, from 42 to six in the ventral column and from 13 to four

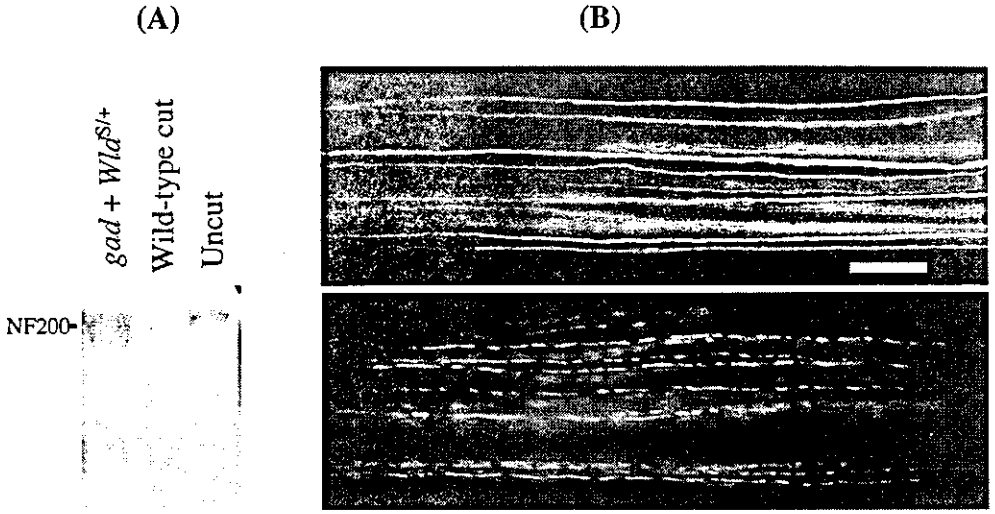

Fig. 1 A single allele of *Wld*^{S} is sufficient to delay Wallerian degeneration even in *gad* mice. **(A)** Western blot showing complete preservation of intact heavy neurofilament protein (NF200) in the distal stump of axotomized *gad* sciatic nerve by heterozygous *Wld*^{S} 5 days after lesion (lane 1). In contrast, no intact NF200 remains after 5 days in axotomized wild-type sciatic nerve (lane 2). Lane 3 is an uncut nerve showing the expected appearance of intact NF200 (gel loading differences probably account for the difference in intensity with lane 1). **(B)** Complete preservation of distal *gad* tibial nerve by heterozygous *Wld*^{S} 5 days after nerve lesion (upper panel), visualized using the *YFP-H* transgene. In contrast, no unfragmented axons remained in a tibial nerve lacking *Wld*^{S} 3 days after a lesion (lower panel). Unlesioned nerves appear exactly as in the upper image (Beirowski *et al.*, 2004). Scale bar = 100 μm.

in the dorsal horn grey matter. Although lumbar regions of only a single *gad* and two *gad/Wld*^{S} mice were studied, these mice were independent of those used for the gracile tract analysis and 3 weeks younger, so these data independently support our conclusion that *Wld*^{S} reduces axonal spheroid pathology in several different regions of *gad* CNS well into late-stage disease.

A reduction in the number of axonal spheroids could result theoretically from either reduced axon pathology or pathology so extensive that the axons are completely destroyed. Kurihara *et al.* (2001) reported that when *gad* pathology was made worse by crossing with *Uch-l3* null mice, extensive axon pathology became detectable at more caudal locations in cervical and thoracic gracile fascicle. We did not observe this in the *Wld*^{S} cross, and *Wld*^{S} homozygotes maintain a rostral–caudal gradient of axonal spheroid pathology (Fig. 2E and F; and thoracic data not shown), indicating that *gad* remains a 'dying-back' pathology in *Wld*^{S} mice but that its progress is delayed.

Secondary measures of axon pathology are also reduced by Wld^S

Further evidence of a reduced loss of axon-myelin units in *gad/Wld*^{S} mice came from a significant reduction ($P = 0.018$) in secondary myelin loss in cervical gracile fascicle in the same animals (Fig. 3A–C). A similar protective trend in the medulla oblongata did not reach statistical significance ($P = 0.059$), probably due to the naturally weaker myelination in this region, but *Wld*^{S} clearly did not cause any deterioration, so the reduction in axonal spheroid numbers (Fig. 2) must reflect reduced pathology and not wholesale axon loss. Furthermore, as the rescued axons remain myelinated, they potentially retain normal conductance properties, at least in these locations. It is unlikely that *Wld*^{S} has any direct effect on myelin, because expression of *Wld*^{S} in glia does not alter Wallerian degeneration (Glass *et al.*, 1993). Thus reduced myelin loss in *gad/Wld*^{S} mice is likely to reflect the maintenance of functional axon-myelin units. *Wld*^{S} also decreased GFAP signal in immunocytochemistry in *gad*, indicating a lower level of astrocyte activation in response to axon damage (Yamazaki *et al.*, 1988) (data not shown). Thus, both direct and indirect measures of spheroidal axon pathology in the gracile tract are reduced by the *Wld*^{S} gene.

Wld^S *operates downstream of axonal ubiquitin depletion in gad*

gad causes axon degeneration through defective ubiquitin metabolism (Osaka *et al.*, 2003), and *Wld*^{S} also interferes with ubiquitin metabolism (Mack *et al.*, 2001; Coleman and Perry, 2002; Zhai *et al.*, 2003). It was important to establish whether *Wld*^{S} blocks the ubiquitin defect in *gad*, an action that would suggest a protective effect restricted to *gad* and other ubiquitin defects, or whether it acts on a downstream step, raising the possibility of delaying axonal spheroid pathology in a wide range of CNS disorders (see above). Interpretation of any change in ubiquitin level in gracile tract would be complicated by the degeneration of those axon branches, so instead we carried out immunocytochemistry for ubiquitin epitopes in the peripheral branch of the same axons in sciatic nerve (Fig. 4). First, we confirmed that axonal ubiquitin was severely depleted in *gad* mice compared with wild-type controls ($P = 0.014$) (Osaka *et al.*, 2003). We then found

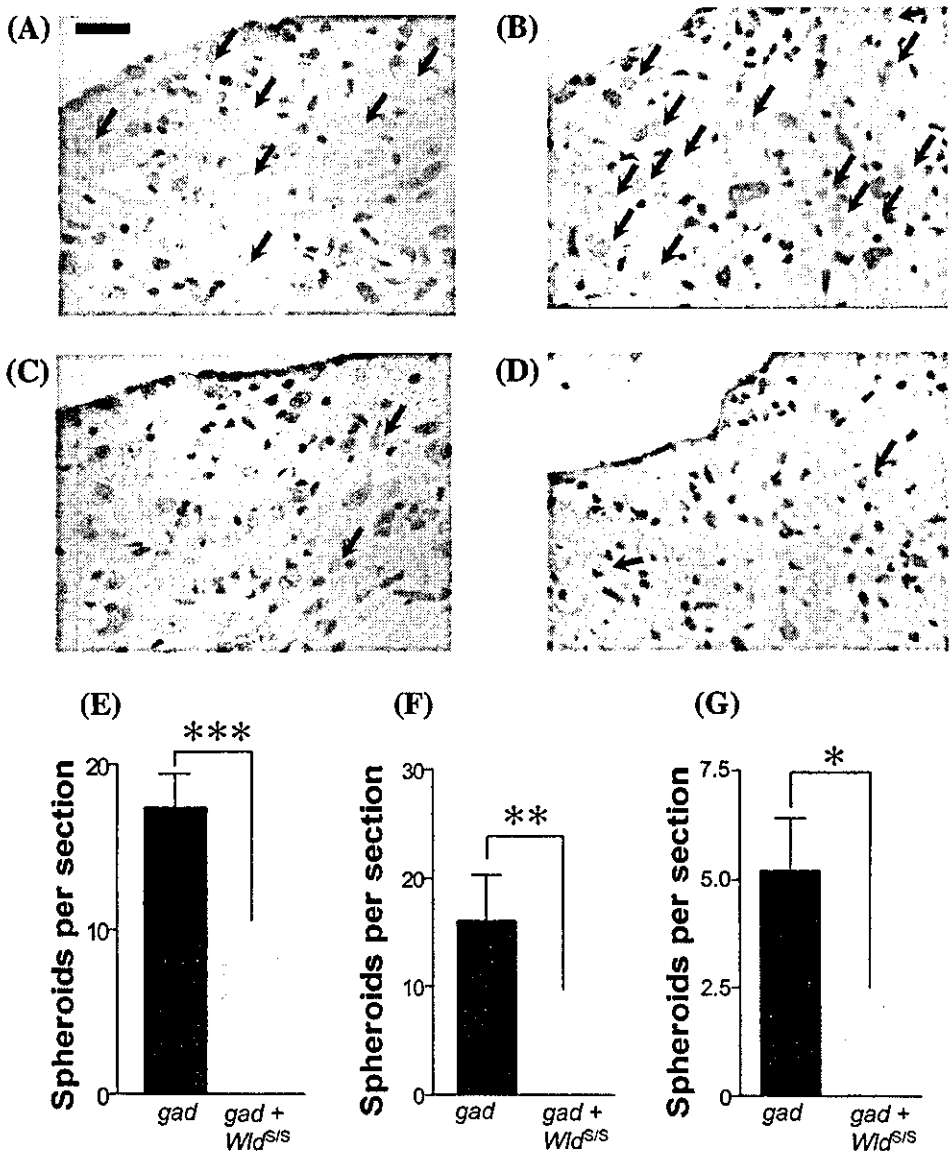

Fig. 2 *Wld*^{S} reduces spheroid body numbers in the gracile tract and lateral columns of *gad* mice. (**A** and **C**) Representative sections from gracile nucleus of (**A**) *gad* and (**C**) *gad/Wld*^{S} mice stained with H & E, showing a large reduction in the number of axonal spheroids (large pink swellings, indicated by arrows) when *Wld*^{S} is present. (**B** and **D**) Representative sections from cervical gracile fascicle of (**B**) *gad* and (**D**) *gad/Wld*^{S} mice. Scale bar (**A–D**) = 25 μm. (**E–G**) Quantitation (mean ± SD) of spheroid counting data in (**E**) gracile nucleus (n = 6), (**F**) cervical gracile fascicle (n = 6) and (**G**) cervical lateral columns (n = 3). *P < 0.05; **P < 0.01; ***P < 0.001.

that a similar defect was present in *gad/Wld*^{S} mice compared with *Wld*^{S} controls (P = 0.0004) and that *Wld*^{S} did not significantly increase the ubiquitin signal either in the presence (P = 0.902) or absence (P = 0.807) of *gad*. Thus, *Wld*^{S} does not correct the depletion of axonal ubiquitin in *gad* and instead operates at a downstream point in spheroid pathology that could be common to other CNS disorders.

Motor pathology

Despite the reduction in axonal spheroids in the gracile tract, there was no apparent reduction in the severity of *gad* symptoms when *Wld*^{S} was present, with no significant difference in hindlimb clasping, (P = 0.82; n = 9) or splay test (P = 0.33; n = 7). Thus, either prevention of swelling in the gracile tract does not preserve the function of those axons, or pathology elsewhere limits any improvement in phenotype of *gad/Wld*^{S} mice. In the absence of any tests to specifically target the function of gracile tract axons, we investigated neuromuscular junction (NMJ) pathology, where dying-back of motor nerve terminals has previously been reported (Miura *et al.*, 1993). At 15 weeks, the degree of denervation was similar between the two strains, with 56.0 ± 6.0% of lumbrical NMJ fully or partially denervated in *gad* mice and 53.5 ± 11.8% in *gad/Wld*^{S} (Fig. 5C and D). This may be because protection of motor nerve terminals at the NMJ by *Wld*^{S} after axotomy is weaker than that of the axon trunk, especially in older mice (Gillingwater *et al.*, 2002). However,

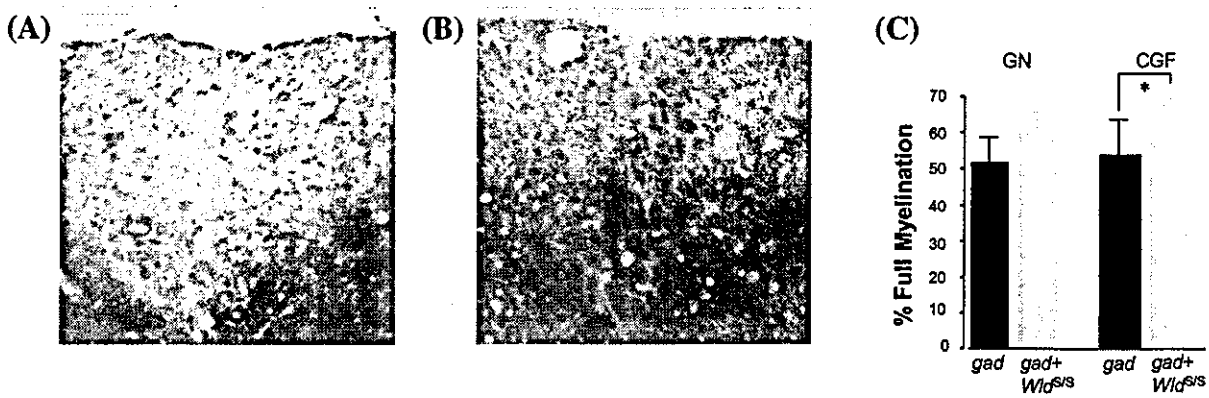

Fig. 3 *Wld*^{S} reduces also secondary demyelination in the gracile tract. (**A** and **B**) Representative cervical gracile fascicles of (**A**) *gad* and (**B**) *gad/Wld*^{S} mice stained with Luxol Fast Blue and Nuclear Fast Red, showing the reduction in myelin loss when *Wld*^{S} is present. Scale bar (**A** and **B**) = 25 μm. (**C**) Densitometric quantification (mean ± SD) of Luxol Fast Blue staining (n = 5). *P < 0.05.

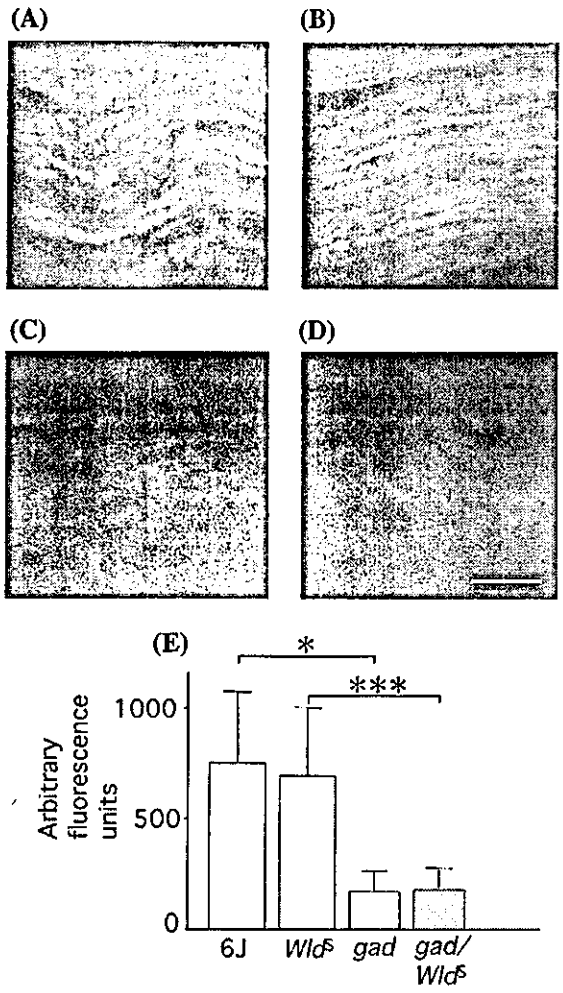

Fig. 4 *Wld*^{S} does not correct the severe depletion of axonal ubiquitin in *gad*. Ubiquitin immunostaining in both (**A**) wild-type and (**B**) *Wld*^{S} mice is greatly reduced in **C** and **D**, respectively, where *gad* is also present. Comparison of **A** with **B** and **C** with **D** also shows that *Wld*^{S} does not alter ubiquitin signal either in the presence of absence of *gad*. (**E**) Quantitation (mean ± SD) of ubiquitin signal. *P < 0.05; ***P < 0.001. 6 J, n = 4; *Wld*^{S}, n = 4; *gad*, n = 4; and *gad/Wld*^{S}, n = 10. Scale bar = 50 μm.

at 9 weeks, an age where *Wld*^{S} does protect axotomized motor nerve terminals, neither strain showed any denervation of NMJ in lumbrical muscles (Fig. 5A and B), so there was no time window when both *Wld*^{S} and *gad* exert their opposing effects at the NMJ. Thus, the fact that *Wld*^{S} does not alleviate NMJ pathology in the older mice could explain why *gad* symptoms are not reduced.

Discussion

We report that *Wld*^{S} reduces the occurrence of axonal spheroids in *gad*. This is the first indication that *Wld*^{S} can alleviate axon pathology in chronic CNS disease, thus extending observations made in the PNS that *Wld*^{S} protects axons not only after injury (Lunn *et al.*, 1989) but also in disorders where no physical injury takes place (Wang *et al.*, 2002; Ferri *et al.*, 2003; Samsam *et al.*, 2003). We conclude that axonal spheroid pathology in *gad* and Wallerian degeneration are not independent events and axon degeneration mechanisms are more uniform than morphology would suggest. It follows that Wallerian degeneration, or processes related to it, could contribute to many other CNS disorders where its involvement has not previously been suspected.

The mechanism by which *Wld*^{S} protects axons is still under investigation (Mack *et al.*, 2001; Coleman and Perry, 2002; Zhai *et al.*, 2003; Araki *et al.*, 2004), but appears to involve nuclear Wld^S protein and a factor(s) that communicates its effect to the axon. What is already becoming clear, however, is that *Wld*^{S} directly or indirectly blocks a central step of axon pathology onto which various pathological mechanisms converge (Fig. 6). This is indicated both by the wide range of disorders in which *Wld*^{S} protects axons, as it is inconceivable that *Wld*^{S} blocks different initial events in each case, and by our direct evidence, that early steps of *gad* pathogenesis are unaltered (Fig. 4). Intriguingly, it now seems that a number of different pathological manifestations result from the step delayed by *Wld*^{S}. These are axonal spheroids in *gad*, dying-back axon loss without swelling in peripheral

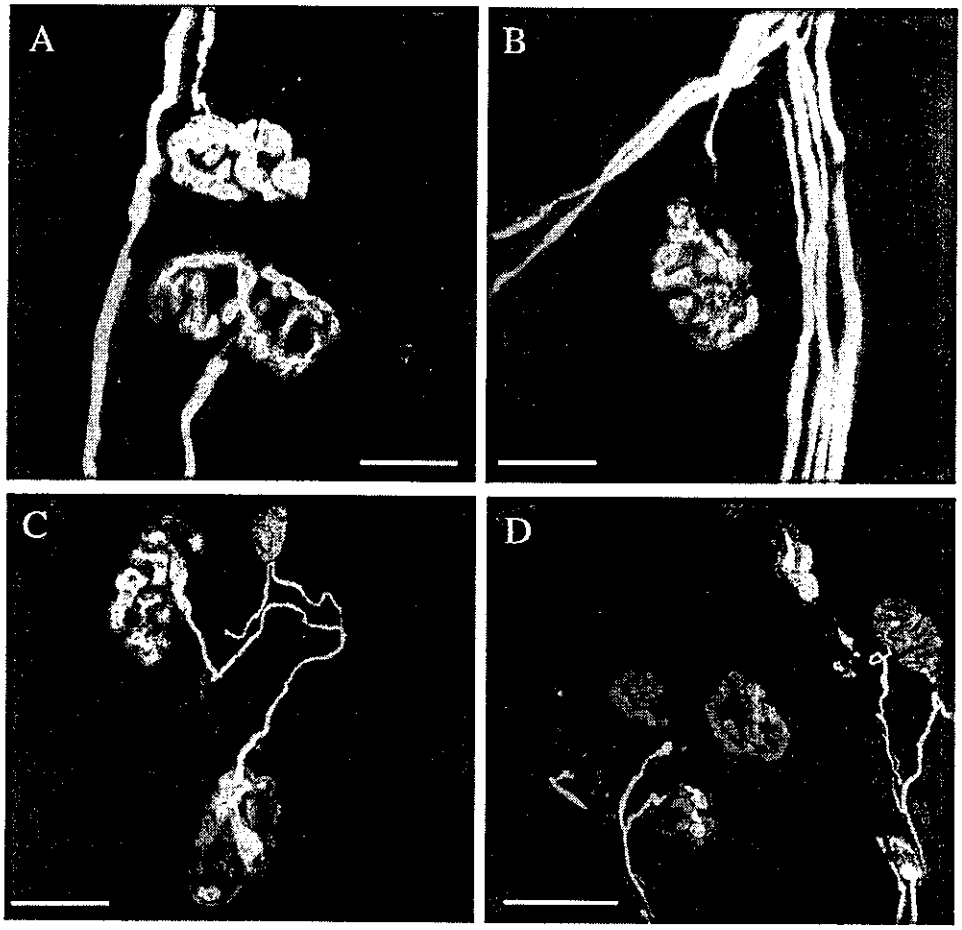

Fig. 5 Denervation at the NMJ. Presynaptic structures labelled with SV2 and neurofilament antibody are shown in green, and postsynaptic structures labelled with TRITC-α-bungarotoxin are in red. At 9 weeks, denervation has hardly begun in (**A**) *gad* or (**B**) *gad*/*Wld*^{S}. At 15 weeks, both strains show extensive denervation (**C** and **D**, respectively), with partial occupancy of endplates by motor nerve terminals occurring frequently. Scale bar = 25 μm.

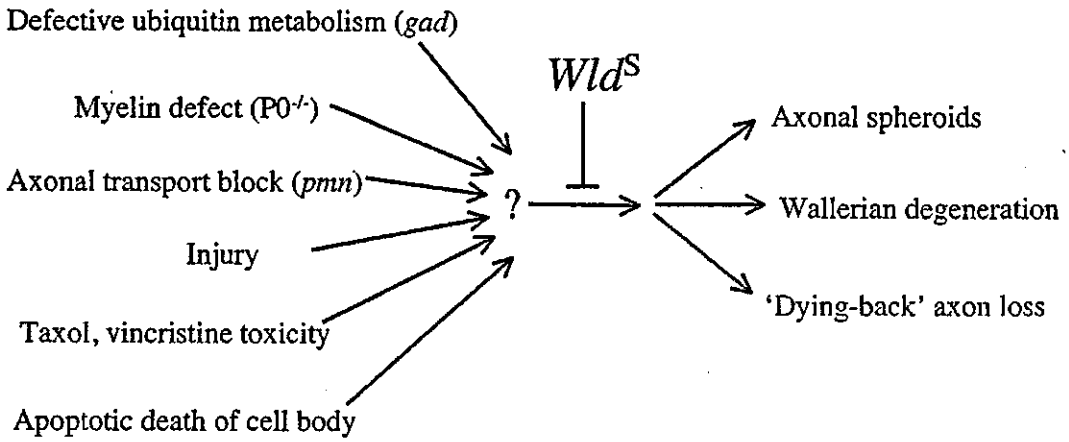

Fig. 6 *Wld*^{S} delays a central step of axonal pathology that lies after the convergence point of multiple degenerative stimuli but upstream of the divergence of several pathological manifestations.

neuropathy and motor neuronopathy, and Wallerian degeneration in CNS and PNS injury. The divergent morphology and topology in these disorders previously suggested independent mechanisms, but the results of directly probing the mechanism using *Wld*^{S} challenge this interpretation.

Many CNS disorders in which there is axonal swelling show accumulation of amyloid precursor protein in the swellings,

indicating impairment of axonal transport in each case and suggesting that their axon degeneration mechanisms are to some extent related. *gad* is one of these disorders, and the others include brain trauma (Gentleman *et al.*, 1993), stroke (Dewar *et al.*, 1999) and other forms of ischaemia (Hughes *et al.*, 2003), multiple sclerosis (Ferguson *et al.*, 1997), and HIV dementia (Medana and Esiri, 2003). This similarity with *gad* suggests that axon degeneration in other disorders may also be related to Wallerian degeneration, a possibility that should now be tested using Wld^S mice or, where appropriate, the newly generated Wld^S rat model (Adalbert *et al.*, in press). However, it is unlikely that Wld^S will stop all forms of axonal swelling, as it appears unable to do so in *Plp* null mice (Edgar *et al.*, 2004). Thus, it should be possible to categorize CNS axonal swelling disorders into those that are altered by Wld^S and those that are not. This will then enable disorders to be grouped together for mechanistic studies rather than focusing on each disorder in isolation.

It is important to consider the spatial and temporal relationship between axonal swelling and axonal breakdown in the light of our data. The lack of good methods for longitudinal imaging of CNS axons has made it difficult to determine whether spheroids first occur as terminal endbulbs of axons whose distal ends have degenerated, or as localized swellings on otherwise morphologically normal axons. Preliminary data from our laboratory using axons of *gad*/YFP-H mice (Adalbert and Coleman., unpublished) suggest that many spheroids in *gad* are not terminal endbulbs, at least in the early stages of the disease. Thus, one model to account for the effect of Wld^S in *gad* is that an 'en passant' spheroid is the first step in pathology, leading to degeneration of the distal axon due to the blockage of axonal transport, a process that fixes the spheroid as a terminal endbulb. In this model, Wld^S might block the Wallerian-like degeneration of the distal end for long enough to allow the spheroid to resolve and the axon to recover. Thus, our data suggest that Wld^S could be used to address the question of whether swollen axons can recover or whether they are destined, inevitably, to degenerate. In a wider context, this is an important issue in several CNS disorders where axonal spheroids occur, including brain trauma and multiple sclerosis (Cheng and Povlishock, 1988; Ferguson *et al.*, 1997).

The above model assumes that Wallerian-like degeneration and axonal swelling in *gad* are separated in space and time, with one causing the other. Alternatively, the mechanism of the axonal swelling itself in *gad* may be related to that of Wallerian degeneration. In support of this model, there are a number of disorders in which CNS axons swell and PNS axons of the same animal degenerate by Wallerian-like degeneration without extensive swelling. In *gad* mice, this occurs even within the same cell, as gracile tract central projections of lumbar primary sensory neurons have spheroids, while peripheral muscle spindles degenerate without swelling (Oda *et al.*, 1992). Similarly, amyotrophic lateral sclerosis (ALS) in humans (Tu *et al.*, 1996; Takahashi *et al.*, 1997), mice (Tu *et al.*, 1996; Oosthuyse *et al.*, 2001) and rats (Howland *et al.*, 2002), together with tauopathy in mice (Lewis *et al.*, 2000; Probst *et al.*, 2000), all show axonal swelling in spinal cord and other CNS areas, but extensive 'Wallerian-like' degeneration without swelling in ventral roots and peripheral nerves. Even injury-induced Wallerian degeneration shows different morphology depending on experimental circumstances. For example, when injured gracile tract axons undergo Wallerian degeneration they swell to up to 10 times their normal diameter, quite unlike Wallerian degeneration in the PNS (George and Griffin, 1994). Thus, a number of observations support a direct mechanistic link between axonal swelling and Wallerian degeneration.

It is not yet clear how related mechanisms might cause swelling in spheroids but axon fragmentation in Wallerian degeneration. Cytoskeletal changes are common to both, so a loosening of cytoskeletal structure could cause disorganized cytoskeleton to accumulate in spheroids but to undergo rapid granular disintegration in Wallerian degeneration. Wallerian degeneration of injured gracile tract axons displays elements of both processes, possibly having an intermediate mechanism: like spheroids, these axons dilate considerably but, typical of Wallerian degeneration, they also rapidly lose their cytoskeletal proteins (George and Griffin, 1994). In traumatic brain injury, observation of Wallerian degeneration and spheroids in the same transverse thin section has been interpreted as degenerating axons having a more proximal spheroid that blocks axonal transport (Cheng and Povlishock, 1988). In view of our findings, an additional explanation needs to be considered, that spheroids and Wallerian degeneration are alternative responses of different axons to the same lesion. Methods for real-time or long-range longitudinal analysis of individual spheroid-containing axons are required to resolve this, similar to new methods already applicable in PNS axons (Pan *et al.*, 2003; Beirowski *et al.*, 2004). What determines whether an axon develops a spheroid or undergoes Wallerian degeneration? Possible explanations include the different glial and haematopoietic cell content of the CNS and the lower rate of axonal transport there (Wujek and Lasek, 1983), but injury type may also be important. Finally, since the discovery of the Wld^S mouse, Wallerian degeneration is no longer considered a passive wasting of distal axons but a regulated self-destruction programme (Buckmaster *et al.*, 1995; Raff *et al.*, 2002). The reduction of axonal spheroid pathology in *gad* by the same gene raises similar questions: rather than being a passive consequence of blocked axonal transport axonal swelling could be, like Wallerian degeneration, a programmed response to axon damage.

Altered ubiquitin metabolism plays important roles in neurodegenerative diseases of the CNS. Genetic mutations in Parkinson's disease include an E3 ligase (Kitada *et al.*, 1998) and possibly *UCH-L1*, the human homologue of the gene mutated in *gad* (Leroy *et al.*, 1998). Ubiquitin-positive inclusions and other evidence indicate abnormal ubiquitylation in Alzheimer's disease (Mori *et al.*, 1987;

van Leeuwen *et al.*, 1998), polyglutamine disorders (DiFiglia *et al.*, 1997; Cummings *et al.*, 1999; Bence *et al.*, 2001) and ALS (Tu *et al.*, 1996; Bruijn *et al.*, 1997). Axons and synapses are particularly vulnerable, as proteasome inhibitors cause specific degeneration of distal neurites (Laser *et al.*, 2003) and ubiquitin-related mutations alter synapse growth (DiAntonio *et al.*, 2001) and stability (Wilson *et al.*, 2002). As *Wld*^{S} can counter a downstream effect of defective ubiquitin metabolism, it now becomes important to study its effects on the above disorders.

Wld^S did not alleviate the symptoms of *gad* mice. Unfortunately, methods do not currently exist to assess the function of gracile tract axons, so we cannot rule out the possibility that blocking spheroid formation did not preserve axon function. However, it is likely that continued neuromuscular pathology in *gad/Wld*^{S} mice also contributes to the symptoms. These mice suffered extensive synapse loss by 15 weeks (Fig. 5), whereas axon pathology was still strongly reduced 3 weeks later (Fig. 2). This supports the hypothesis that different mechanisms underlie synaptic and axonal degeneration, with *Wld*^{S} affording only limited protection to synapses, particularly in older mice (Gillingwater and Ribchester, 2001; Gillingwater *et al.*, 2002). Similarly, the synapses of gracile tract axons may have been lost even when those axons are preserved. Our data suggest that synapse pathology is a limiting factor when axons are protected by *Wld*^{S}, a finding likely to be important in other models (Ferri *et al.*, 2003; Samsam *et al.*, 2003).

In summary, we conclude that *Wld*^{S} alleviates chronic CNS axon pathology in *gad* mice and that formation of distal axonal spheroids in this disease shares features with Wallerian degeneration and 'dying-back' axon loss without spheroids. The effect of *Wld*^{S} on other CNS disorders with ubiquitylation deficits and CNS axonal swelling disorders should now be studied. Finally, our data emphasize the importance of finding a way to protect synapses as strongly as *Wld*^{S} protects axons.

Acknowledgements

We thank Professor Tateki Kikuchi for advice on *gad* pathology, Professor Rudolf Martini (University of Würzburg), Dr Mohtashem Samsam (University of Würzburg and Saba University School of Medicine), Dr Till G. A. Mack (Key Neurotek, Magdeburg, Germany), Dr Martin Bootman (The Babraham Institute, Cambridge) and Ms Jolanta Kozlowski (University of Cologne) for helpful discussion and technical advice. This work was supported by the Federal Ministry of Education and Research (FKZ: 01 KS 9502) and Center for Molecular Medicine, University of Cologne (CMMC) (to W.M., B.B., R.A., D.W., D.G. and M.P.C.), the Wellcome Trust (to T.H.G., plus Biomedical Collaboration Grant to R.R.R. and M.P.C), the Biotechnology and Biological Sciences Research Council (M.P.C., R.A., L.C.), ALSA (R.A.), the Koeln Fortune Programme (B.B.), the Grants-in-Aid for Scientific Research from the Ministry of Education, Culture, Sports, Science and Technology of Japan (K.W.) and from the Ministry of Health, Labour and Welfare of Japan (K.W.).

References

Adelbert R, Gillingwater TM, Haley JE, Bridge K, Beirowski B, Berek L, Wagner D, Grumme D, Thomson D, Celik A, Addicks K, Ribchester RR, and Coleman MP. A rat model of slow Wallerian degeneration (Wld^S) with improved preservation of synapses. Eur J Neurosci. In press.

Adle-Biassette H, Chretien F, Wingertsmann L, Hery C, Ereau T, Scaravilli F, et al. Neuronal apoptosis does not correlate with dementia in HIV infection but is related to microglial activation and axonal damage. Neuropathol Appl Neurobiol 1999; 25: 123–33.

Araki T, Sasaki Y, Milbrandt H. Increase nuclear NAD biosynthesis and SIRT1 activation prevent axonal degeneration. Science 2004; 305: 1010–3.

Beirowski B, Berek L, Adalbert R, Wagner D, Grumme DS, Addicks K, et al. Quantitative and qualitative analysis of Wallerian degeneration using restricted axonal labeling in YFP-H mice. J Neurosci Methods 2004; 134: 23–35.

Bence NF, Sampat RM, Kopito RR. Impairment of the ubiquitin–proteasome system by protein aggregation. Science 2001; 292: 1552–5.

Bomont P, Cavalier L, Blondeau F, Ben Hamida C, Belal S, Tazir M, et al. The gene encoding gigaxonin, a new member of the cytoskeletal BTB/kelch repeat family, is mutated in giant axonal neuropathy. Nat Genet 2000; 26: 370–4.

Brendza RP, O'Brien C, Simmons K, McKeel DW, Bales KR, Paul SM, et al. PDAPP;YFP double transgenic mice: a tool to study amyloid-b associated changes in axonal, dendritic and synaptic structures. J Comp Neurol 2003; 456: 375–83.

Bruijn LI, Becher MW, Lee MK, Anderson KL, Jenkins NA, Copeland NG, et al. ALS-linked SOD1 mutant G85R mediates damage to astrocytes and promotes rapidly progressive disease with SOD1-containing inclusions. Neuron 1997; 18: 327–38.

Bu B, Li J, Davies P, Vincent I. Deregulation of cdk5, hyperphosphorylation, and cytoskeletal pathology in the Niemann–Pick Type C murine model. J Neurosci 2002; 22: 6515–25.

Buckmaster EA, Perry VH, Brown MC. The rate of Wallerian degeneration in cultured neurons from wild type and C57BL/Wld^S mice depends on time in culture and may be extended in the presence of elevated K^+ levels. Eur J Neurosci 1995; 7: 1596–602.

Cheng CLY, Povlishock JT. The effect of traumatic brain injury on the visual system: a morphologic characterization of reactive axonal change. J Neurotrauma 1988; 5: 47–60.

Coleman MP, Perry VH. Axon pathology in neurological disease: a neglected therapeutic target. Trends Neurosci 2002; 25: 532–7.

Coleman MP, Conforti L, Buckmaster EA, Tarlton A, Ewing RM, Brown MC, et al. An 85-kb tandem triplication in the slow Wallerian degeneration (Wld^S) mouse. Proc Natl Acad Sci USA 1998; 95: 9985–90.

Conforti L, Tarlton A, Mack TG, Mi W, Buckmaster EA, Wagner D, et al. A Ufd2/D4Cole1e chimeric protein and overexpression of Rbp7 in the slow Wallerian degeneration (Wld^S) mouse. Proc Natl Acad Sci USA 2000; 97: 11377–82.

Cummings CJ, Reinstein E, Sun Y, Antalffy B, Jiang Y, Ciechanover A, et al. Mutation of the E6-AP ubiquitin ligase reduces nuclear inclusion frequency while accelerating polyglutamine-induced pathology in SCA1 mice. Neuron 1999; 24: 879–92.

Dewar D, Yam P, McCulloch J. Drug development for stroke: importance of protecting cerebral white matter. Eur J Pharmacol 1999; 375: 41–50.

DiAntonio A, Haghighi AP, Portman SL, Lee JD, Amaranto AM, Goodman CS. Ubiquitination-dependent mechanisms regulate synaptic growth and function. Nature 2001; 412: 449–52.

DiFiglia M, Sapp E, Chase KO, Davies SW, Bates GP, Vonsattel JP, et al. Aggregation of huntingtin in neuronal intranuclear inclusions and dystrophic neurites in brain. Science 1997; 277: 1990–3.

Edgar JM, McLaughlin M, Yool D, Zhang SC, Fowler JH, Montague P, et al. Oligodendroglial modulation of fast axonal transport in a mouse model of hereditary spastic paraplegia. J Cell Biol 2004; 166: 121–31.

Feng G, Mellor RH, Bernstein M, Keller-Peck C, Nguyen QT, Wallace M, et al. Imaging neuronal subsets in transgenic mice expressing multiple spectral variants of GFP. Neuron 2000; 28: 41–51.

Ferguson B, Matyszak MK, Esiri MM, Perry VH. Axonal damage in acute multiple sclerosis lesions. Brain 1997; 120: 393–9.

Ferreirinha F, Quattrini A, Pirozzi M, Valsecchi V, Dina G, Broccoli V, et al. Axonal degeneration in paraplegin-deficient mice is associated with abnormal mitochondria and impairment of axonal transport. J Clin Invest 2004; 113: 231–42.

Ferri A, Sanes JR, Coleman MP, Cunningham JM, Kato AC. Inhibiting axon degeneration and synapse loss attenuates apoptosis and disease progression in a mouse model of motoneuron disease. Curr Biol 2003; 13: 1–20.

Galvin JE, Uryu K, Lee VM, Trojanowski JQ. Axon pathology in Parkinson's disease and Lewy body dementia contains alpha-, beta-, and gamma-synuclein. Proc Natl Acad Sci USA 1999; 96: 13450–5.

Gentleman SM, Nash MJ, Sweeting CJ, Graham DI, Roberts GW. Beta-amyloid precursor protein (beta APP) as a marker for axonal injury after head injury. Neurosci Lett 1993; 160: 139–44.

George R, Griffin JW. The proximo-distal spread of axonal degeneration in the dorsal columns of the rat. J Neurocytol 1994; 23: 657–67.

Gillingwater TH, Ribchester RR. Compartmental neurodegeneration and synaptic plasticity in the Wld^S mutant mouse. J Physiol 2001; 534: 627–39.

Gillingwater TH, Thomson D, Mack TG, Soffin EM, Mattison RJ, Coleman MP, et al. Age-dependent synapse withdrawal at axotomised neuromuscular junctions in Wld^S mutant and Ube4b/Nmnat transgenic mice. J Physiol 2002; 543: 739–55.

Gillingwater TH, Haley JE, Ribchester RR, Horsburgh K. Neuroprotection after transient global cerebral ischemia in Wld(s) mutant mice. J Cereb Blood Flow Metab 2004; 24: 62–6.

Glass JD, Brushart TM, George EB, Griffin JW. Prolonged survival of transected nerve fibres in C57BL/Ola mice is an intrinsic characteristic of the axon. J Neurocytol 1993; 22: 311–21.

Griffiths I, Klugmann M, Anderson T, Yool D, Thomson C, Schwab MH, et al. Axonal swellings and degeneration in mice lacking the major proteolipid of myelin. Science 1998; 280: 1610–3.

Howland DS, Liu J, She Y, Goad B, Maragakis NJ, Kim B, et al. Focal loss of the glutamate transporter EAAT2 in a transgenic rat model of SOD1 mutant-mediated amyotrophic lateral sclerosis (ALS). Proc Natl Acad Sci USA 2002; 99: 1604–9.

Hughes PM, Anthony DC, Ruddin M, Botham MS, Rankine EL, Sablone M, et al. Focal lesions in the rat central nervous system induced by endothelin-1. J Neuropathol Exp Neurol 2003; 62: 1276–86.

Ichihara N, Wu J, Chui DH, Yamazaki K, Wakabayashi T, Kikuchi T. Axonal degeneration promotes abnormal accumulation of amyloid beta-protein in ascending gracile tract of gracile axonal dystrophy (GAD) mouse. Brain Res 1995; 695: 173–8.

Kikuchi T, Mukoyama M, Yamazaki K, Moriya H. Axonal degeneration of ascending sensory neurons in gracile axonal dystrophy mutant mouse. Acta Neuropathol (Berl) 1990; 80: 145–51.

Kitada T, Asakawa S, Hattori N, Matsumino H, Yamamura Y, Minoshima S, et al. Mutations in the parkin gene cause autosomal recessive juvenile parkinsonism. Nature 1998; 392: 605–8.

Kornek B, Storch MK, Weissert R, Wallstroem E, Stefferl A, Olsson T, et al. Multiple sclerosis and chronic autoimmune encephalomyelitis: a comparative quantitative study of axonal injury in active, inactive, and remyelinated lesions. Am J Pathol 2000; 157: 267–76.

Kornek B, Storch MK, Bauer J, Djamshidian A, Weissert R, Wallstroem E, et al. Distribution of a calcium channel subunit in dystrophic axons in multiple sclerosis and experimental autoimmune encephalomyelitis. Brain 2001; 124: 1114–24.

Kurihara LJ, Kikuchi T, Wada K, Tilghman SM. Loss of Uch-L1 and Uch-L3 leads to neurodegeneration, posterior paralysis and dysphagia. Hum Mol Genet 2001; 10: 1963–70.

Laser H, Mack TGA, Wagner D, Coleman MP. Proteasome inhibition arrests neurite outgrowth and causes 'dying-back' degeneration in primary culture. J Neurosci Res 2003; 15: 906–16.

Leroy E, Boyer R, Auburger G, Leube B, Ulm G, Mezey E, et al. The ubiquitin pathway in Parkinson's disease. Nature 1998; 395: 451–2.

Lewis J, McGowan E, Rockwood J, Melrose H, Nacharaju P, Van Slegtenhorst M, et al. Neurofibrillary tangles, amyotrophy and progressive motor disturbance in mice expressing mutant (P301L) tau protein. Nat Genet 2000; 25: 402–5.

Liberski PP, Budka H. Neuroaxonal pathology in Creutzfeldt-Jakob disease. Acta Neuropathol (Berl) 1999; 97: 329–34.

Lunn ER, Perry VH, Brown MC, Rosen H, Gordon S. Absence of Wallerian degeneration does not hinder regeneration in peripheral nerve. Eur J Neurosci 1989; 1: 27–33.

Mack TG, Reiner M, Beirowski B, Mi W, Emanuelli M, Wagner D, et al. Wallerian degeneration of injured axons and synapses is delayed by a Ube4b/Nmnat chimeric gene. Nat Neurosci 2001; 4: 1199–206.

Medana IM, Esiri MM. Axonal damage: a key predictor of outcome in human CNS diseases. Brain 2003; 126: 515–30.

Mi W, Conforti L, Coleman MP. Genotyping methods to detect a unique neuroprotective factor (Wld^S) for axons. J Neurosci Methods 2002; 113: 215–8.

Mi W, Glass JDG, Coleman MP. Stable inheritance of an 85-kb triplication in C57BL/Wld^S mice. Mut Res 2003; 526: 33–7.

Miike T, Ohtani Y, Nishiyama S, Matsuda I. Pathology of skeletal muscle and intramuscular nerves in infantile neuroaxonal dystrophy. Acta Neuropathol (Berl) 1986; 69: 117–23.

Miura H, Oda K, Endo C, Yamazaki K, Shibasaki H, Kikuchi T. Progressive degeneration of motor nerve terminals in gad mutant mouse with hereditary sensory axonopathy. Neuropathol Appl Neurobiol 1993; 19: 41–51.

Mori H, Kondo J, Ihara Y. Ubiquitin is a component of paired helical filaments in Alzheimer's disease. Science 1987; 235: 1641–4.

Mukoyama M, Yamazaki K, Kikuchi T, Tomita T. Neuropathology of gracile axonal dystrophy (gad) mouse. Acta Neuropathol 1989; 79: 294–9.

Norreel JC, Jamon M, Riviere G, Passage E, Fontes M, Clarac F. Behavioural profiling of a murine Charcot–Marie–Tooth disease type 1A model. Eur J Neurosci 2001; 13: 1625–34.

Oda K, Yamazaki K, Miura H, Shibasaki H, Kikuchi T. Dying back type axonal degeneration of sensory nerve terminals in muscle spindles of the gracile axonal dystrophy (gad) mutant mouse. Neuropathol Appl Neurobiol 1992; 18: 265–81.

Oosthuyse B, Moons L, Storkebaum E, Beck H, Nuyens D, Brusselmans K, et al. Deletion of the hypoxia-response element in the vascular endothelial growth factor promoter causes motor neuron degeneration. Nat Genet 2001; 28: 131–8.

Osaka H, Wang Y-L, Takada K, Takizawa S, Setsuie R, Li H, et al. Ubiquitin carboxy-terminal hydrolase L1 binds to and stabilises monoubiquitin in neurons. Hum Mol Genet 2003; 12: 1945–58.

Pan YA, Misgeld T, Lichtman JW, Sanes JR. Effects of neurotoxic and neuroprotective agents on peripheral nerve regeneration assayed by time-lapse imaging *in vivo*. J Neurosci 2003; 23: 11479–88.

Probst A, Gotz J, Wiederhold KH, Tolnay M, Mistl C, Jaton AL, et al. Axonopathy and amyotrophy in mice transgenic for human four-repeat tau protein. Acta Neuropathol (Berl) 2000; 99: 469–81.

Raff MC, Whitmore AV, Finn JT. Axonal self-destruction and neurodegeneration. Science 2002; 296: 868–71.

Raja F, Sherriff FE, Morris CS, Bridges LR, Esiri MM. Cerebral white matter damage in HIV infection demonstrated using beta-amyloid precursor protein immunoreactivity. Acta Neuropathol (Berl) 1997; 93: 184–9.

Saigoh K, Wang YL, Suh JG, Yamanishi T, Sakai Y, Kiyosawa H, et al. Intragenic deletion in the gene encoding ubiquitin carboxy-terminal hydrolase in gad mice. Nat Genet 1999; 23: 47–51.

Sajadi A, Schneider BL, Aebischer P. Wld^S-mediated protection of dopaminergic fibers in an animal model of Parkinson disease. Curr Biol 2004; 14: 326–30.

Samsam M, Mi W, Wessig C, Zielasek J, Toyka KV, Coleman MP, et al. The Wld^S mutation delays robust loss of motor and sensory axons in a

genetic model for myelin-related axonopathy. J Neurosci 2003; 23: 2833–9.

Sidman RL, Angevine JB, Pierce ET. Atlas of mouse brain and spinal cord. Cambridge: Harvard University Press; 1971.

Sung JH, Mastri AR, Park SH. Axonal dystrophy in the gracile nucleus in children and young adults. J Neuropathol Exp Neurol 1981; 40: 37–45.

Takahashi T, Yagishita S, Amano N, Yamaoka K, Kamei T. Amyotrophic lateral sclerosis with numerous axonal spheroids in the corticospinal tract and massive degeneration of the cortex. Acta Neuropathol (Berl) 1997; 94: 294–9.

Trapp BD, Peterson J, Ransohoff RM, Rudick R, Mork S, Bo L. Axonal transection in the lesions of multiple sclerosis. N Engl J Med 1998; 338: 278–85.

Tu PH, Raju P, Robinson KA, Gurney ME, Trojanowski JQ, Lee VM. Transgenic mice carrying a human mutant superoxide dismutase transgene develop neuronal cytoskeletal pathology resembling human amyotrophic lateral sclerosis lesions. Proc Natl Acad Sci USA 1996; 93: 3155–60.

van Leeuwen FW, de Kleijn DP, van den Hurk HH, Neubauer A, Sonnemans MA, Sluijs JA, et al. Frameshift mutants of beta amyloid precursor protein and ubiquitin-B in Alzheimer's and Down patients. Science 1998; 279: 242–7.

Wang MS, Davis AA, Culver DG, Glass JD. Wld^S mice are resistant to paclitaxel (Taxol) neuropathy. Ann Neurol 2002; 52: 442–7.

Wilson SM, Bhattacharyya B, Rachel RA, Coppola V, Tessarollo L, Householder DB, et al. Synaptic defects in ataxia mice result from a mutation in Usp14, encoding a ubiquitin-specific protease. Nat Genet 2002; 32: 420–5.

Wujek JR, Lasek RJ. Correlation of axonal regeneration and slow component B in two branches of a single axon. J Neurosci 1983; 3: 243–51.

Yamazaki K, Wakasugi N, Tomita T, Kikuchi T, Mukoyama M, Ando K. Gracile axonal dystrophy (gad), a new neurological mutant in the mouse. Proc Soc Exp Biol Med 1988; 187: 209–15.

Zhai Q, Wang J, Kim A, Liu Q, Watts R, Hoopfer E, et al. Involvement of the ubiquitin-proteasome system in the early stages of Wallerian degeneration. Neuron 2003; 39: 217–25.

Journal of Neurochemistry, 2005, 92, 1061–1072 doi:10.1111/j.1471-4159.2004.02963.x

Potentiation of ATP-induced currents due to the activation of P2X receptors by ubiquitin carboxy-terminal hydrolase L1

Yoshimasa Manago,* Yoshiko Kanahori,* Aki Shimada,* Ayumi Sato,* Taiju Amano,* Yae Sato-Sano,*,† Rieko Setsuie,*,† Mikako Sakurai,*,† Shunsuke Aoki,† Yu-Lai Wang,† Hitoshi Osaka,†,‡ Keiji Wada† and Mami Noda‡

**Laboratory of Pathophysiology, Graduate School of Pharmaceutical Sciences, Kyushu University, Fukuoka, Japan*

†Department of Degenerative Neurological Diseases, National Institute of Neuroscience, National Center of Neurology and Psychiatry, Tokyo, Japan

‡Information and Cellular function, PRESTO, Japan Science and Technology Corporation (JST), Kawaguchi, Saitama, Japan

Abstract

Mammalian neuronal cells abundantly express a de-ubiquitinating isozyme, ubiquitin carboxy-terminal hydrolase L1 (UCH L1). Loss of UCH L1 function causes dying-back type of axonal degeneration. However, the function of UCH L1 in neuronal cells remains elusive. Here we show that overexpression of UCH L1 potentiated ATP-induced currents due to the activation of P2X receptors that are widely distributed in the brain and involved in various biological activities including neurosecretion. ATP-induced inward currents were measured in mock-, wild-type or mutant (C90S)-UCH L1-transfected PC12 cells under the conventional whole-cell patch clamp configuration. The amplitude of ATP-induced currents was significantly greater in both wild-type and C90S UCH L1-transfected cells, suggesting that hydrolase activity was not involved but increased level of mono-ubiquitin might play an important role. The increased currents were dependent on cAMP-dependent protein kinase (PKA) and Ca^{2+} and calmodulin-dependent protein kinase (CaMKII) but not protein kinase C. In addition, ATP-induced currents were likely to be modified via dopamine and cyclic AMP-regulated phosphoprotein (DARPP-32) that is regulated by PKA and phosphatases. Our finding shows the first evidence that there is a relationship between UCH L1 and neurotransmitter receptor, suggesting that UCH L1 may play an important role in synaptic activity.

Keywords: CaMKII, DARPP-32, PKA, patch-clamp, PC12, UCH L1.

J. Neurochem. (2005) **92**, 1061–1072.

The ubiquitin-proteasome system is an evolutionarily conserved and energy-dependent proteolytic pathway that functions constitutively to degrade proteins. Recent studies indicate that ubiquitin-mediated proteolysis can also be regulated and is of widespread importance (Wilkinson 1995; Coux *et al.* 1996). Regulated proteolysis by the ubiquitin-

Received August 24, 2004; accepted October 8, 2004.

Address correspondence and reprint requests to Mami Noda, PhD, Laboratory of Pathophysiology, Graduate School of Pharmaceutical Sciences Kyushu University, 3-1-1 Maidashi, Higashi-ku, Fukuoka 812–8582, Japan, Tel./Fax: + 81-92-642-6574.

E-mail: noda@phar.kyushu-u.ac.jp

Abbreviations used: ATP, adenosine triphosphate; BSA, bovine serum albumin; CaMKII, Ca^{2+} and calmodulin-dependent protein kinase; CDK, cyclin-dependent kinase; CHO, cells, Chinese hamster ovary cells; CREB, Ca^{2+}-stimulated cAMP response element binding protein; DAPI, 4′, 6-diamidino-2-phenylindole, dihydrochloride; EGTA, ethyleneglycol-bis-N, N, N′, N′-tetraacetic acid; ERK, extracellular signal-regulated kinase; DARPP-32, dopamine and cyclic AMP-regulated phosphoprotein with molecular weight of about 32 000; 1,9-dideoxyforskolin, 7β-acetoxy-6β-hydroxy-8,13-epoxy-labd-14-en-11-one; FBS, fetal bovine serum; forskolin, 7β-acetoxy-8,13-epoxy-1α,6β,9α-trihydroxy-labd-14-en-11-one; H-89, N-[2-(p-bromoocinamylamino)ethyl]-5-isoquinolinesulfonamide; HS, horse serum; KN-93, 2-[N-(2-hydroxyethyl)]-N-(4-methoxybenzenesulfonyl)]amino-N-(4-chlorocinnamyl)-N-methylbenzylamine); HEPES, N-2-hydroxyethylpiperazine-N′-2-ethansulfonic acid; MAPK, mitogen-activated protein kinase; NGF, nerve growth factor; PBS(–), Dulbecco's Ca^{2+}, Mg^{2+}-free phosphate buffer saline; PC12, cells, rat phenochromocytoma cells; PD98059, 2′-Amino-3′-methoxyflavone; PGP9.5, protein gene product 9.5; PKA, cyclic AMP-dependent protein kinase; PKC, protein kinase C; PP1, protein phosphatase 1; PP2, protein phosphatase 2; SDS-PAGE, sodium dodecyl sulfate-polyacrylamide gel electrophoresis; TBST, Tris buffer saline-Tween; Thr-34, threonine at 34; Thr-75, threonine at 75; Roscovitine, 2-(R)-(1-Ethyl-2-hydroxyethylamino)-6-benzylamino-9-isopropylpurine; UCH, L1, ubiquitin C-terminal hydrolase L1.

proteasome pathway has been implicated in the control of cell cycle (King *et al.* 1996), transcription activation (Verma *et al.* 1995), antigen presentation (Rock *et al.* 1994), cell fate and growth (Huang *et al.* 1995; Zhu *et al.* 1996), synaptogenesis (Muralidhar and Thomas 1993; Oh *et al.* 1994) and memory (Hegde *et al.* 1997). Ubiquitination of proteins is mediated by specific enzymes (E1, E2, and E3) and polyubiquitinated proteins are translocated to the 26S proteasome and subsequently proteolytically degraded (Ciechanover *et al.* 2000). Conversely, deubiquitination is thought to be essential for the regulation of proteolysis and for recycling of monoubiquitin from polyubiquitin chains.

Recently, one of the deubiquitinating enzymes, UCH L1 (ubiquitin carboxy-terminal hydrolase L1), was reported to be essential for brain function. UCH L1 is selectively expressed in neuron and testis (Wilkinson *et al.* 1989; Wilkinson *et al.* 1992). Loss of UCH L1 function was shown to cause neuronal degeneration observed in the gracile axonal dystrophy (*gad*) mouse (Saigoh *et al.* 1999), and missence mutation of UCH L1 was found in familial Parkinson disease (Leroy *et al.* 1998). As physiological functions of UCH L1, it is not limited to hydrolase activity; it has been shown that it associated with mono-ubiquitin and thus stabilized free ubiquitin by preventing its degradation within lysosomes. UCH L1's affinity for ubiquitin rather than hydrolase activity was required for the regulation of ubiquitin level (Osaka *et al.* 2003) and UCH L1 even might work as ubiquitin ligase (Liu *et al.* 2002). Furthermore, UCH L1 has been reported to have an important role in apoptosis in germ cell and neuron (Harada *et al.* 2004; Kwon *et al.* 2004b) and different UCH isozymes have distinct function during spermatogenesis (Kwon *et al.* 2004a).

As for neural function of UCH L1, little is known yet. In *Aplysia*, homologous UCH was shown to be important for learning and memory (Hegde *et al.* 1997). It is not yet known that UCH L1 works in a similar way in mammalian cells, but these results strongly suggest that UCH L1 plays an important role in synaptic function and morphology. In the present study, we investigated the neuronal function of UCH L1 on receptor channels which affect neurotransmitter secretion.

PC12 cells are often used as a model for studying neuronal cell function. Among neurotransmitter receptors expressed in PC12 cells, ATP receptors induce dopamine release (Sela *et al.* 1991). ATP receptors are divided into two subtypes, P2X and P2Y receptors. P2X receptors are ionotropic receptors and form cationic channels, while P2Y receptors are G-protein-coupled receptors and $P2Y_{1,\ 2,\ 4,\ 6,\ 11}$ cause intracellular Ca^{2+} mobilization via IP3 formation and activate Ca^{2+}-dependent K^+ channels (Ikeuchi *et al.* 1996). Among P2X receptors, $P2X_2$ and $P2X_4$ receptor mRNA have been detected in PC 12 cells (Hur *et al.* 2001). P2X receptors mediate fast ionic flow and are supposed to induce depolarization of the cells, hence contributing to the catecholamine release from PC12 cells. Therefore, we first analyzed P2X receptors and their modulation by UCH L1. This is the first report to show a relationship between UCH L1 and neurotransmitter receptors and may help to understand the function of UCH L1 in the nervous system.

Materials and methods

Cell culture

PC12 Tet-off cells were grown in RPMI-1640 medium containing 5% fetal bovine serum (FBS) (Cell Culture Technologies, CANSER INTERNATIONAL INC., Canada), 10% horse serum (HS) (Gibco/BRL, Grand Island, NY, USA), 100 units/mL penicillin (Life Technologies, Rockville, MD, USA) and 100 μg/mL streptomycin (Life Technologies) in a humidified atmosphere with 10% CO_2 at 37°C. To differentiate PC12 Tet-off cells, 100 ng/mL of nerve growth factor (NGF) was added to the RPM1640 medium with 0.1% HS, 0.05% FBS, 50 unit/mL penicillin and 100 μg/mL streptomycin for 4 days.

CHO-AA8-Lucl cells were maintained in Minimum Essential Medium Eagle α modification (Sigma, St Louis, MO, USA) containing 10% FBS, 100 units/mL penicillin, 100 μg/mL streptomycin, and 4 mM L-glutamine (Gibco/BRL), with 10% CO_2 at 37°C.

Transfection

Plasmids used for transfection were constructed using pBI-EGFP Tet vector (Clontech). For electrophysiological recording, PC12 Tet-Off cells were transfected with mock, wild-type or mutant (C90S) human UCH L1 cDNA, using Lipofectamine 2000. After 24 h, PC12 Tet-Off cells were treated with NGF and differentiated for 4–5 days. More precisely, 3.0 × ~10^5/dish PC12 Tet-Off cells were seeded in 35-mm dishes in RPMI with 10% HS and 5% FBS. Twenty-four hours after seeding, the medium was replaced with 500 μL of serum-free RPMI1640 medium. Then, the transfection mixture containing 4 μg of cDNA and 10 μL of Lipofectamine 2000 in 500 μL of RPMI-1640 was added to each dish and incubated for 6 h in a humidified atmosphere with 10% CO_2 at 37°C. One ml of complete RPMI-1640 supplemented with an additional 10% HS and 5% FBS was then added to each dish. The solution for transfection was discarded 18 h later and replaced with RPMI-1640 medium for differentiation with added 100 ng/mL NGF. For protein analysis, CHO-AA8-Lucl cells (7.5 × ~10^5/well, Clontech) were transfected in the same way. After 24 h, cells were subjected to western blot analysis or immunocytochemical analysis.

Western blot analysis

Transfected CHO-AA8-Lucl cells were washed with PBS contained protease inhibitor and after collecting lysates in solution containing 20 mM Tris-base, 0.1% SDS, 1% sodium deoxycholate, 1% Triton X-100 and 0.001 g/5 mL protease inhibitor and then centrifuged at 15 000 r.p.m. for 30 min at 4°C. After collecting supernatant, protein concentrations of lysates were determined using Bio-Rad protein assay kits (Bio-Rad, Hercules, CA, USA). Lysates were boiled for 10 min, resolved by 10–20% gradient SDS-PAGE, and transferred to polyvinylidene difluoride membranes (Bio-Rad) with a semidry electroblotter (Bio-Rad). The membrane was blocked by incubation in 1% BSA/TBST for 1 h at room temperature. Anti-PGP9.5 (UCH L1) antibody (1 : 100, Medac) was used as a primary antibody in Western blotting. Anti-rabbit IgG conjugated with

horseradish peroxidase (1: 2000) (Dako, Carpinteria, CA, USA) was used as secondary antibody. Immunoreactive bands were detected using the supersignal substrate system (Pierce, Rockford, IL, USA) according to manufacturer's instructions.

Immunocytochemical analysis

After transfection, cells were fixed with 4% paraformaldehyde. Immunocytochemistry on CHO-AA8-LucI cells and PC12 Tet-Off cells was performed as previously described (Osaka *et al.* 2003) using antibodies to ubiquitin that is predominantly reactive to free ubiuitin in immuno-histochemistry (1 : 100, Sigma; polyclonal) and UCH L1 (1 : 100, Medac; monoclonal). For immunofluorescence studies, antirabbit IgG conjugated with Cy3 antibodies (1 : 200, Jackson Immuno Research) and antirabbit IgG conjugated with Alexa Fluor 568 antibodies (1 : 1000, Molecular Probes) were used as secondary antibodies. Also, in PC12 Tet-Off cells, 300 μM DAPI was applied to stain transfected and untransfected cell nuclei for 5 min, and then the cells were washed with PBS for 5 min at least five times. Twenty confocal images with 0.5 μm width were obtained and reconstructed using the confocal laser microscope system (Radiance2100, Bio-Rad). To stain mono-ubiquitin, the same laser strength was used in mock, wild-type and C90S UCH L1-transfeacted cells under the confocal laser microscope system (LSM510, Carl Zeiss, Germany).

Electrophysiological measurements

The cell with fluorescence was chosen under the fluorescence microscope. Then, the patch pipette was applied to the cell to obtain a giga-ohm seal under the phase bright mode. Whole-cell recordings were made as reported previously (Noda *et al.* 1999, 2000), using an Axopatch-200B amplifier (Axon Instruments, Foster City, CA, USA), under voltage-clamp condition at the holding potential of −70 mV. Membrane currents were measured using a patch pipette containing (in mM): CsCl, 120; Mg_2ATP_3, 3; HEPES, 20; $CaCl_2$, 1; $MgCl_2$, 1; EGTA, 5. The pH of the solution was adjusted to 7.2 with 1 N CsOH. The pipette resistance was 5–9 MΩ. The external solution contained (mM): NaCl, 132; KCl, 5; $CaCl_2$, 2; $MgCl_2$, 1; glucose, 10; and HEPES, 10. The pH was adjusted to 7.4 with 1 N NaOH. External ATP or drugs were applied rapidly using the 'Y tube' technique (Min *et al.* 1996), which allows the complete exchange of the external solution surrounding a cell within 20 ms. Temperature monitored in the recording dishes was 33–34°C.

In the experiments using inhibitors except PD98059, ATP was applied twice to ensure reproducibility of the ATP-induced current in control experiments. The inhibitor solution was applied after first application of ATP for the period according to the references for each inhibitor until the end of second application of ATP. The current amplitude obtained at the second application of ATP with or without inhibitors normalized to the first ATP-induced current. All values were presented as means ± SEM. Statistical analysis was done using ANOVA. A value of $p < 0.05$ was considered to be the minimum level of significance. Curve fitting was performed using Hill Equation (Igor Pro 4.07; Wavemetrics, Lake Oswego, OR, USA).

SYBR Green-based Real-Time Quantitative RT–PCR

Total RNAs were prepared from 2×10^6 PC12 Tet-Off cells and a rat brain with RNeasy™. RNA purification kit (QIAGEN, Valencia, CA, USA) according to the manufacturer's protocol. First-strand cDNA synthesized from 1 μg total RNA with random hexamer primers was used as template for each reaction. SYBR Green-based Real-time Quantitative RT-PCR was performed as described (Wong *et al.* 2000; Aoki *et al.* 2002). Applied Biosystems 7700 Sequence Detection System was used for the signal detection and the PCR was performed in 1 × SYBR Green Master mix (Applied Biosystems, Foster City, CA, USA) and 50 nM of each primer. For standardization and quantification, rat β-actin or rat glyceraldehyde 3-phosphate dehydrogenase (GAPDH) was amplified simultaneously. Primer sequences were designed with Primer Express™ Software (Applied Biosystems). The following primer pairs were employed: 5′-TGCAGACCATCAGCAACCTG-3′ (upper, 17–36) and 5′-CTTGTGGATACCCCAGCTCC-3′ (lower, 103–84) for amplification of rat DARPP-32 (primer set A; GenBank accession No. AF281661): 5′-CACCTGCAGACCATCAGCAA-3′ (upper, 13–32) and 5′-CCTCTTGTGGATACCCCAGC-3′ (lower, 106–87) for amplification of rat DARPP-32 (primer set B; AF281661): 5′- ATCGCTGACAGGATGCAGAAG-3′ (upper, 925–945) and 5′-AGAGCCACCAATCCACACAGA-3′ (lower, 1032–1012) for amplification of rat β-actin: and 5′-ACCACAGTCCATGCCATCAC-3′ (upper, 586–605) and 5′- TCCACCACCCTGTTGCTGTA-3′ (lower, 1037–1018) for amplification of rat GAPDH. PCR conditions were: 95°C for 10 min, followed by 40 cycles at 95°C for 15 s and 60°C for 1 min. The threshold cycle of each gene was determined as the PCR cycle at which an increase in fluorescence was observed above the baseline signal in an amplification plot (Wada *et al.* 2000). The 'normalized expression level of target' (dCt) was calculated as the difference in threshold cycles for target and reference (β-actin or GAPDH). Subtraction of dCt for PC12 Tet-Off cells from dCt for the rat brain provided the ddCt value. The formula, 2^{-ddCt}, was used to calculate relative expression levels for PC12 Tet-Off cells compared to the rat brain. To reduce possible error, RT-PCR reaction was performed three times and averaged 2^{-ddCt} values were obtained. In addition, two gene-specific primer sets (set A and B, see above) for DARPP-32 gene and two independent RNA pools were examined to confirm DARPP-32 gene expression.

Drugs and reagents

RPMI-1640 medium, ATP-2Na, H-89, chelerythrine, roscovitine, PD98059, forskolin and 1,9-dideoxyforskolin were from SIGMA (St. Louis, MO, USA). NGF and Lipofectamine 2000 were from Gibco/BRL (Grand Island, NY, USA). KN-93 and okadaic acid was from CALBIOCHEM (San Diego, CA, USA).

Results

Transfection of UCH L1 in PC12 Tet-Off cells

Expression activity of plasmid constructs was first examined in CHO-AA8-LucI cells that lack endogenous expression of UCH L1 (Fig. 1). Confocal microscopic examination revealed that UCH L1 immunoreactivity colocalizes with GFP fluorescence (Fig. 1a). Western blot analysis showed bands immunostained by anti-UCH L1 antibodies were

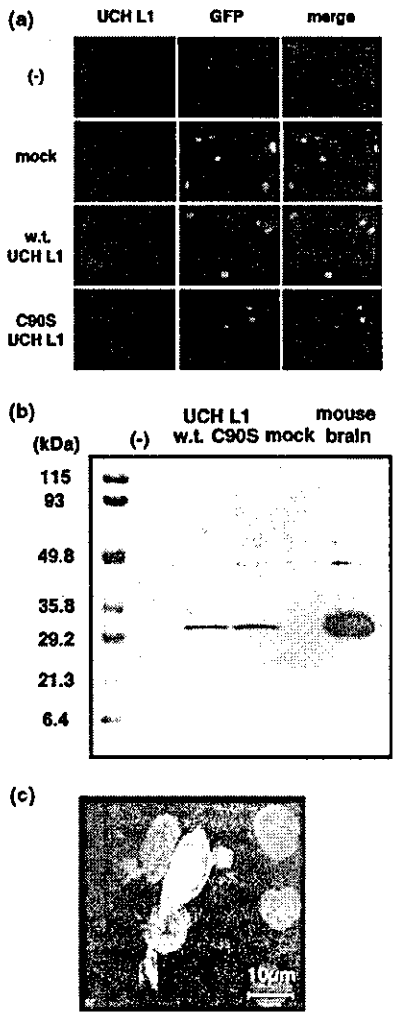

Fig. 1 Transfection efficacy of UCH L1 in CHO-AA8-Lucl cells and PC12 Tet-Off cells. (a) Confocal image of CHO-AA8-Lucl cells 24 h after transfection of pBI-EGFP-mock, wild type UCH L1 and C90S UCH L1 with Lipofectamine 2000 were double stained with UCH L1 (red). Cells with green fluorescence (GFP) are the transfected cells. (b) Western-blot analysis of CHO-AA8-Lucl cells 24 h after transfection of pBI-EGFP-mock, -wild type UCH L1 and -C90S UCH L1 with Lipofectamine 2000. CHO-AA8-Lucl cells were lysed with TBS buffer containing 0.1% Triton X. 10 μg of each protein was subjected to SDS-PAGE and immunoblotted with anti-PGP9.5 antibody. (c) Confocal image of overexpressed UCH L1 in PC12 Tet-Off cells were double stained with GFP (green) and DAPI (blue).

detected in cells transfected with pBI-EGFP-wild type UCH L1 or C90S UCH L1, but not mock plasmids (Fig. 1b). Figure 1(c) shows a PC12 Tet-Off representative cell with green fluorescence used for electrophysiological recording, although DAPI staining was not employed for the recording. The efficacy of the transfection was about 10% in PC12 Tet-Off cells.

Effects of overexpression of UCH L1 on ATP-induced currents

ATP-activated inward currents due to the activation of P2X receptors at the negative holding potential in PC12 cells were reported (Nakazawa *et al.* 1994). In our experiments, PC12 Tet-Off cells were voltage clamped at −70 mV and high concentration of ATP were used to see whether or not overexpression of UCH L1 affected maximum inward currents. In UCH L1-transfected PC12 Tet-Off cells, ATP-induced inward currents were significantly larger than those in mock-transfected cells. Unexpectedly the mutant (C90S) UCH L1, which lacks C-terminal hydrolase activity but retains ubiquitin binding affinity, had a similar effect to wild-type UCH L1 (Fig. 2a). The amplitude of peak inward currents in mock-, wild-type UCH L1- and C90S UCH L1-transfected PC12 Tet-Off cells were 15.0 ± 1.6 pA/pF ($n = 5$), 48.5 ± 6.0 pA/pF ($n = 6$) and 47.6 ± 4.1 pA/pF ($n = 6$), respectively (Fig. 2b).

The current-voltage relationships of ATP-induced inward currents were analyzed by applying voltage steps of 10 mV increments between −100 mV and + 50 mV with 50 ms duration and 50 ms interval from the holding potential of −70 mV before and during the application of ATP (Fig. 3a). The current traces before and after application of ATP in wild-type UCH L1-transfected PC12 Tet-Off cells were shown by applying voltage steps (Fig. 3b). Holding currents were negligibly misaligned even during the application of ATP. The current levels at the end of each pulse before and during ATP application were obtained in mock-, wild-type UCH L1- or C90S UCH L1-transfected PC12 Tet-Off cells.

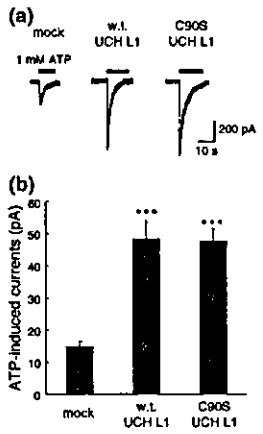

Fig. 2 Current amplitudes of ATP-induced currents in mock-, wild-type UCH L1- and C90S UCH L1-transfected PC12 Tet-Off cells. (a) Inward membrane currents induced by 1 mM ATP at the holding potential of −70 mV in mock-, wild-type (wt) and C90S UCH L1-transfected PC12 Tet-Off cells. (b) Amplitudes of peak inward currents induced by 1 mM ATP in mock-, wild-type and C90S UCH L1-transfected PC12 Tet-Off cells. The bars represent the mean ± SEM. ***: $p < 0.001$.